Summer 2011

Altering Nitric Oxide Bioavailability and Lipid Profiles in Endothelial Cells By Polycyclic Aromatic Hydrocarbons in Particulate Matter

Liang Yu
Old Dominion University

ALTERING NITRIC OXIDE BIOAVAILABILITY AND LIPID

PROFILES IN ENDOTHELIAL CELLS BY POLYCYCLIC

AROMATIC HYDROCARBONS IN PARTICULATE MATTER

by

Liang Yu
B.S. July 2004, Beijing Institute of Technology, China
M.S. July 2006, Beijing Institute of Technology, China

A Dissertation Submitted to the Faculty of
Old Dominion University in Partial Fulfillment of the
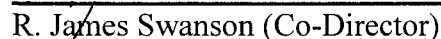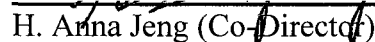Requirements for the Degree of

DOCTOR OF PHILOSOPHY
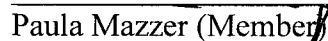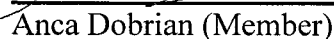
BIOMEDICAL SCIENCES

OLD DOMINION UNIVERSITY
August 2011

Approved by:

R. James Swanson (Co-Director)

H. Anna Jeng (Co-Director)

Paula Mazzer (Member)

Anca Dobrian (Member)

ABSTRACT

ALTERING NITRIC OXIDE BIOAVAILABILITY AND LIPID PROFILES IN ENDOTHELIAL CELLS BY POLYCYCLIC AROMATIC HYDROCARBONS IN PARTICULATE MATTER

Liang Yu
Old Dominion University, 2011
Co-Directors: Dr. R. James Swanson
Dr. H. Anna Jeng

Epidemiologic studies have demonstrated a significant association between exposure to particulate matter (PM) and atherosclerosis. Polycyclic aromatic hydrocarbons (PAHs) present in particulate matter, are well known to induce oxidative stress and lipid peroxidation via generation of reactive oxygen species (ROS). Lipid peroxidation involves regulating endothelial nitric oxide synthase via inhibition of its activity, and as a result, mediates dilation of coronary arterioles is involved with the pathogenesis of atherosclerosis. However, data on assessment of oxidized lipid formation is limited due to low resolution of mass spectrometer methods. Taking the advantage of a Fourier Transform Ion Cyclotron Resonance Mass Spectrometer (FT-ICR-MS) with 12 Tesla at Old Dominion University, this study assessed how lipid peroxidation induced by PAHs altered the lipid profile and nitric oxide level in human endothelial cells.

Human coronary artery endothelial cells (HCAEC) were exposed to PAHs with various doses and treatment duration times. After exposure, the level of ROS was measured using the fluorometric method with a flow cytometer. Lipid peroxidation was assessed based on the formation of malondialdehyde. Nitric oxide synthase was

calculated using a cell-permeable diacetate that reacts with NO to form a fluorescent triazolofluorescein. Then, lipids of HCAEC were extracted by chloroform and methanol and analyzed using 12T FT-ICR-MS to separate peaks.

After PAH exposure, cell morphology noticeably changed, granularity increased, and viability decreased after the short term treatment. The ROS level, expressed as fluorescent intensity readings from a flow cytometer, significantly increased along with the malondialdehyde levels. The analysis of spectrum data from FT-ICR-MS showed changes of the cellular lipid profile in the exposed groups as compared to the control. We found no significant impacts of oxidative stress on nitric oxide bioavailability in endothelial cells. However, direct exposure of HCAEC to PAHs increased lipid oxidization. These data imply that PAHs may mediate nitric oxide synthase activity through lipid peroxidation by a mechanism yet to be elucidated. These studies demonstrate one potential means by which oxidative stress can induce endothelial cell damage and lipid peroxidation during atherosclerosis for a short term exposure.

In conclusion, the oxidation pathway induced by PAHs contributed to endothelial cell damage. This study identified lipids and developed novel data analytic approaches that are applicable in revealing oxidative lipid formation induced by PAHs. In addition, the technology enables us to identify specifically oxidized phospholipids that could serve as biomarkers in assessing PAH-induced endothelial dysfunction and the underlying mechanism.

This thesis is dedicated to my parents, Yaoguang Yu and Lirong Wei, for their unselfish

sacrifice, dedication, support and love throughout the completion of this degree, without

which this study was not possible.

ACKNOWLEDGMENTS

I would like to extend my great appreciation and gratitude to my adviser, Dr. R. James Swanson, for all the mentoring, support, knowledge and this amazing opportunity that he has given me.

I am grateful to my research mentor, Dr. Anna Jeng, for her enthusiastic, inspirational and patient guidance, and the important role she has played in the development of my scientific career.

I would like to thank Dr. Paula Mazzer for taking the time out of her schedule to train me on lipid analysis, and allowing me to use the equipment from her lab.

It is a pleasure to acknowledge and thank Dr. Anca Dobrian for her advice, input and help throughout this project.

I would also like to thank Dr. Gene Hou for all of his support and encouragement throughout my studies at Old Dominion University.

There are many individuals who have been instrumental to the completion of this project through valuable resources, discussions, suggestions, support and time who I would like to acknowledge. Special thanks and gratitude goes to Fang Li, Yiling Chen, Jie Liu, Hongmei Chen, Wei Ren, Dorothy Yordt, Roberto Mendez, Dr. Xinhua Chen, Dr. Yu Jing, Dr. Wentia Ford, and my other friends, my colleagues within the lab and the Department of Biology for all their support.

TABLE OF CONTENTS

LIST OF TABLES

LIST OF FIGURES

CHAPTER I

BACKGROUND, SPECIFIC AIMS, SIGNIFICANCE

BACKGROUND

Particulate Matters

Airborne PM is grouped with diameter sizes range from nanometers to 100 μm. Particles between 10 and 2.5 μm are classified as coarse (PM_{10}), between 2.5 and 0.1 μm are classified as fine ($PM_{2.5}$), less than 0.1 μm are classified as ultrafine (UFP). Exposure to PM is an important public health issue because of its association with cardiovascular mortality and morbidity (Pope and Dockery 2006; Laden et al. 2006; Woodruff et al. 2008). Cardiovascular incidents from PM exposure have increased emergency room use (Schwartz 1999, 2001). Also, the number of PM-associated deaths from cardiovascular disease (CVD) equals or exceeds the number of such deaths from respiratory causes (Peters et al. 1997). More recently, Miller and his colleagues found a 76% increase in cardiovascular mortality for every 10 $\mu g/m^3$ rise in the annual average of airborne fine particulate matter (Miller et al. 2007). Chronic exposure to $PM_{2.5}$ and UFPs increased the severity of atherosclerotic aortic lesions in Watanabe rabbits and apolipoprotein (apo) E-null mice (Chen and Nadziejko 2005; Sun et al. 2005). In human studies involving 798 residents of the Los Angeles basin, Kunzli et al. found a 5.9% increase in the carotid artery intima-media thickness per 10 $\mu g/m^3$ increase in ambient $PM_{2.5}$ (Kunzli et al. 2005).

Some studies showed that the toxicity and the carcinogenicity of PM are related to their size, represent their capabilities to penetrate into the gas-exchange region of the

lungs (Brown et al. 2001). Churg and co-workers found that the adverse health effects appear to correlate better with $PM_{2.5}$ than with PM_{10} concentration (Churg and Brauer 2000). Moreover, electron microscopy analysis showed that 96% of the effectively retained particles in the lung parenchyma were $PM_{2.5}$, while only 5% were ultrafine particles (Churg and Brauer 1997). A study, investigating the association between air pollution and cardiorespiratory health during the winter of 1998-1999 in Amsterdam, the Netherlands, concluded that $PM_{2.5}$ was more strongly related to cardiorespiratory symptoms than PM_{10} and ultrafine particles were (de Hartog et al. 2003).

The importance of the effects of smaller particles on health is recognized by scientific and regulatory communities. The Environmental Protection Agency (EPA) initiated routine monitoring of $PM_{2.5}$ and established new standards for $PM_{2.5}$ under the national ambient air quality standards (NAAQS) in 1997 (EPA 1997). Furthermore, a recent World Health Organization report from panel studies suggested that fine particles (<2.5 µm) are more hazardous than coarse particles in terms of mortality and cardiovascular endpoints. More importantly, additional research is needed to establish the link between ultrafine PM exposure and risks to health in a more accurate and precise manner (WHO 2003).

To date, there is limited data elucidating biological mechanisms between $PM_{2.5}$ exposure and acute events of cardiovascular disease. Thus, this proposed study's aim is to confirm the toxicity effects of $PM_{2.5}$ and assess whether polycyclic aromatic hydrocarbons (PAHs) is a major component contribute to cytotoxicity in endothelium in relation to pathogenesis of cardiovascular disease.

Polycyclic Aromatic Hydrocarbons

The use of diesel engine powered vehicles has been increasing in all over the world with an increased need for transportation, and hence proportional higher indexes of air pollution (Sydbom et al. 2001). Diesel engines emit more nitrogen oxides and particles than gasoline engines though they offer better fuel efficiency and lower emissions of carbon dioxide (Hesterberg et al. 2006). Fuel combustion and diesel engine powered vehicle are the primary source for PM. The respirable diesel exhaust particles (DEP) provide a good absorption surface for incomplete combustion derivatives of diesel engines, on which an estimated 18000 different organic compounds such as PAHs, nitro aromatic hydrocarbons, heteocyclics, quinones, aldehydes, and aliphatic hydrocarbons (Salvi and Holgate 1999; Bai et al. 2001). Among them, article-bound PAHs are one of major chemical components of PM and have been evaluated as potential carcinogens and mutagens and precipitate the development of several diseases (Kavouras and Stephanou 2002).

PAHs are a group of over 100 different chemicals. Pure PAHs usually exist as colorless, white, or pale yellow-green solids that are formed during the incomplete burning of coal, oil and gas, garbage, or other organic substances like tobacco or charbroiled meat. Structure of representative PAH compounds are showed in Figure 1.
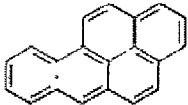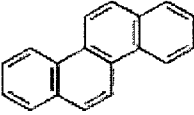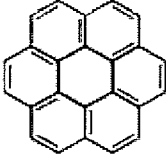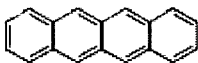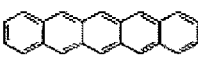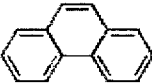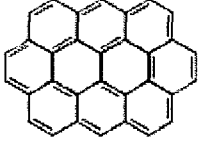
Chemical compound		Chemical compound	
Anthracene		Benzo[a]pyrene	
Chrysene		Coronene	
Corannulene		Tetracene	
Naphthalene		Pentacene	
Phenanthrene		Pyrene	
Triphenylene		Ovalene	

Figure 1. Structure of PAH compounds (EPA 2008).

The United States Environmental Protection Agency (EPA) has designated 16 PAH compounds as priority pollutants. They are naphthalene, acenaphthylene, acenaphthene, fluorene, phenanthrene, anthracene, fluoranthene, pyrene, benzo[a]anthracene, chrysene, benzo[b]fluoranthene, benzo[k]flouranthene, benzo[a]pyrene, dibenz(ah)anthracene, benzo[ghi]perylene, and indeno(1,2,3-cd)pyrene (Lunch 2005). The 16 EPA priority PAHs are often targeted for measurement in environmental samples. Although the health effects of individual PAHs are not exactly alike, the Agency for Toxic Substances and Disease Registry (ATSDR) has issued a PAH

profile as a group for their carcinogenic mutagenic and teratogenic properties. (ATSDR 1995). The Occupational Safety and Health Administration (OSHA) have set a limit of 0.2 milligrams of PAHs per cubic meter of air with the consideration to protect workers' health. The OSHA Permissible Exposure Limit for mineral oil mist that contains PAHs is 5 mg/m^3 averaged over an 8-hour exposure period (Rothberg et al.). The National Institute for Occupational Safety and Health (NIOSH) recommends that the average workplace air levels for coal tar products not exceed 0.1 mg/m^3 for a 10-hour workday, within a 40-hour workweek (ATSDR 1995).

Oxidative Stress

Oxidative stress is a general term that characterizes the imbalance by an increase in pro-oxidant species and/or a decrease in anti-oxidant defense that occur during oxidative metabolism in biologic systems. Oxidative stress has been suggested as a major mechanism in biological effects induced by PM (Cruts et al. 2008; Li et al. 2008). Human studies have associated increased systemic oxidative stress with exposure to PM$_{2.5}$ with elevation in plasma levels of thiobarbituric acid reactive substances (TBARS) of 28 nonsmoking seniors (Liu et al. 2009). This result is in agreement with earlier reports of increased serum TBARS in association with PM$_{2.5}$ (Sorensen et al. 2003). Experimental animal work brings support to the causality notion. Gong has reported that exposure to the PM$_{2.5}$ and UFP led to increased hepatic lipid peroxidation, accompanied by a higher up regulation of Nrf2-regulated antioxidant genes in the mouse livers (Gong et al. 2007).

PAHs have been speculated as one of the components of PM inducing oxidative stress. In humans, the PAHs biotransformation process begins with a cytochrome P450-mediated epoxidation of the chemical to become electrophilic intermediates (Georgellis et al. 1990). These reactive intermediates are then capable of engaging in redox cycling and produce reactive oxygen species (ROS).

ROS are cellular oxidants which include free radicals such as superoxide ($O_2^-\cdot$), hydroxyl (OH$\cdot$) and peroxyl (ROO$\cdot$), as well as non-radical species such as hydrogen peroxide (H_2O_2). These oxidizing species are common by-products of several cellular processes including aerobic metabolism, fatty acid oxidation, cytochrome P450 activity, and the respiratory burst of immune cells (Wiseman and Halliwell 1996). Radiation exposure can also lead to the formation of cellular ROS (Limoli et al. 2001).

Cells can posses a number of antioxidant defense mechanisms to protect against the constant generation of ROS, including non-enzymatic scavengers such as glutathione, uric acid, ascorbic acid and α-tocopherol, as well as the enzymes superoxide dismutase (SOD), catalase (CAT), and glutathione peroxidase (GPx). In addition, proteins such as transferrin, metallothionein and ceruloplasmin may act indirectly as antioxidants by sequestering transition metals responsible for the generation of hydroxyl radicals (Salganik 2001). The fact that all ROS would be completely removed by these antioxidant defenses, indicate that ROS may play an important role in cellular functions and that antioxidants exist primarily to maintain a steady state of ROS (Sanders 2005). A study of particulate pollutants showed that UFP, collected in Los Angeles area, were used to study the generation of ROS which caused oxidative stress in macrophages and epithelial cells, and in turn induces pulmonary inflammation. This result confirmed that

UFP induced GSH reduction and resulting in cell toxicity (Li et al. 2003). Therefore, in the event that ROS greatly exceed the antioxidant capabilities of the cell, either by increased generation of ROS or decreased capability of antioxidant defenses, a condition termed oxidative stress results (Davies 2000).

ROS plays a critical role in endothelial activation and potentially cause endothelial dysfunction. Endothelial cell death or injury may contribute to the initial endothelial physiological processes, such as angiogenesis, atherosclerosis, and thrombosis. Previous studies have indicated that the vascular endothelium was sensitive to ROS that can cause cell damage and death. PM_{10} and $PM_{2.5}$ from Mexico City were reported to induce endothelial activation and result in alternation of ROS and apoptosis in human umbilical vein endothelial cells (Montiel-Davalos et al. 2010).

Lipid Peroxidation

ROS is capable of oxidizing damaging macromolecules, including DNA proteins and lipids (Burcham 1999). A study conducted from the coke oven workers showed that chronic exposure to PAHs may induced oxidative stress and lipid peroxidation in blood serum (Jeng et al. 2010). This association between PAHs exposure and oxidative stress was supported by the measurement of molodeadhyde that was accessed as the parameter of lipid peroxidation among 120 school children (Bae et al. 2010).

Lipid peroxidation causes bioactive lipid peroxides formation, which can further oxidize other macromolecules including other fatty acids within membranes (Meerson et al. 1982). Oxidized phospholipids can also initiate and modulate many cellular events that attribute to atherosclerosis, which suggests oxidized phospholipids would serve a biomarker for cardiovascular diseases (Ashraf et al. 2009). Polyunsaturated fatty acids

play a role of frequent targets of ROS and their susceptibility to oxidation increases with their degree of unsaturation (Mates and Sanchez-Jimenez 2000). Long chain PUFAs with more than five double bonds are at greater risk of oxidation than PUFAs with fewer double bonds, such as linoleic acid. Therefore, lipid peroxidation increases particular concerns within cellular membranes when peroxide propagation is not terminated by antioxidants, which can result in large-scale damage to the membrane. Recent studies demonstrated that lipid peroxidation play an important role in the activation of endothelial cells. For example, Ashraf detected two specific phospholipids, 1-palmitoyl-2-(5-oxovaleroyl)-sn-glycero-3-phosphatidylcholine (POVPC), and 1-palmitoyl-2-glutaroylsn-glycero-3-phosphatidylcholine (PGPC) that were involved with the activation of endothelial cells cells (Ashraf et al. 2009). Also, a study assessing oxidized low-density lipoprotein (oxLDL) indicated that lipid peroxidation decrease NO bioavailability which mediate dilation of isolated coronary arterioles (Hein et al. 2000). Subsequent studies confirmed the effect via inhibition of the activity of eNOS. (Uittenbogaard et al. 2000; Shaul 2003).

Phospholipid changes induced by lipid peroxidation yield a large number of oxidation products with different structures, which difficult their isolation and characterization (Domingues et al. 2008). Mass spectrometry using the ionization methods is becoming increasingly important in the study of oxidized lipids. Particularly, ultrahigh resolution techniques such as electrospray ionization (ESI) coupled to Fourier Transform Ion Cyclotron Resonance Mass Spectrometer (FT-ICR-MS) have significantly advanced the knowledge of lipid identification and lipid profiling.

Endothelial Dysfunction

The primary mode of entry into the body is through the respiratory system;

however, the greatest public risk from the air pollution is due to cardiovascular disease

based on the epidemiological data (EPA 2004). An increased incidence of adverse

cardiovascular events has been reported in subjects with impaired endothelial function

compared with subjects with vascular changes, such as decreased vasodilatation,

development of prothrombotic and proinflammatory states and smooth muscle cell

proliferation, all of which contribute to the formation of progression of chronic

atherosclerotic lesions (Bonetti et al. 2003; Libby et al. 2002; Widlansky et al. 2003).

Aging, hypertension, atherosclerosis are important risk factors of stroke and

cardiovascular diseases and seem to be associated with endothelial dysfunction

(Schneider et al. 2008).

The vascular endothelium is important for maintaining vascular homeostasis,

which provides a barrier between the circulation and the surrounding tissues and

contributes in several ways to the local regulation of vascular tone by producing relaxing

and contracting factors. It is known that PM result in increase of ROS in endothelium

(Montiel-Davalos et al. 2010; Delfino et al. 2005). It is also known that ROS reduce

nitric oxide (NO) bioavailability and cause endothelial dysfunction that result in many

non-PM induced cardiovascular diseases (Ohtani and Egashira 2004; Bitar et al. 2005).

In general, PM_{10} can enter the upper large branches of the lung, while smaller particles,

such as $PM_{2.5}$ can enter the bronchial tubes and penetrate deep to the alveolar portion of

the lung. The solvable $PM_{2.5}$, such as PAHs, as well as UFPs may reach the

cardiovascular vessel through blood circulation, in which highly reactive ions or

molecules known as ROS are produced. Because of the presence of unpaired valence

shell electrons, ROS are easily attack biological targets that include protein, lipids, and

DNA. Figure 2 shows that PM-derived ROS may play a critical role in endothelial activation and potentially cause endothelial dysfunction.

NO, an endothelial-derived relaxing factor (EDRF) is believed to be associated with endothelial dysfunction. Lack of NO can increase blood pressure and decrease coronary flow. On the other hand, excess of NO can cause irregular heartbeat. NO is synthesized endogenously from L-Arginine by various NO synthase (NOS) and released to smooth muscle cells to regulate vascular relaxation (Figure 3). In the heart, endothelial NOS (eNOs) is the major form of NOS (Stewart et al. 2009) and is expressed in cardiac myotytes (Samii 2003), suggesting that eNOS is of importance to regulate NO synthesis in the cardiovascular system.
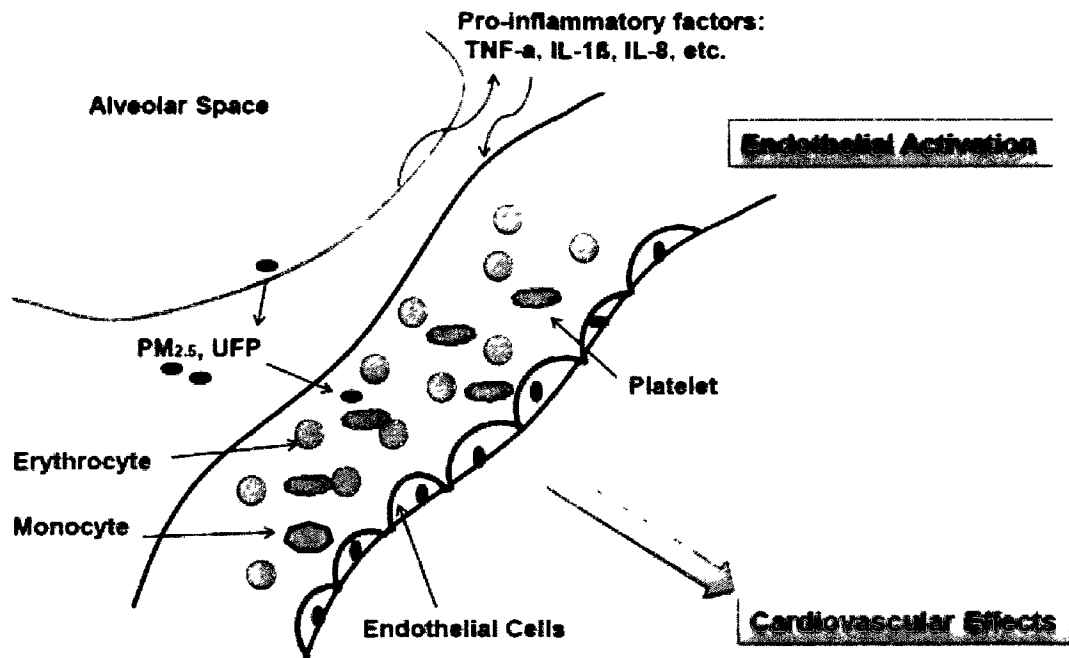
Figure 2. Systemic effects after PM exposure.

Though the mechanisms as how PM cause CVDs are not fully known, several studies have demonstrated that PM can independently cause CVDs in both *in vivo* and *in vitro* model*s* (Polichetti et al. 2009). Figure 4 illustrates possible mechanisms related to PM induced CVDs :

1.   The exposure of PM to the epithelial cells initiates oxidative stress and inflammation by the generation of ROS. The derivatives of the inflammatory cells may enter the cardiovascular system through blood circulation. The damage of the tissue may sicken the patients with previous cardiovascular diseases.

2. $PM_{2.5}$ and ultrafine particles can directly pass to the cardiovascular vessel and contact or penetrate the endothelial cells. These PM can generate ROS, lipid oxidation and alter the NO bioavailability. Such endothelium dysfunction causes hypertension and other cardiovascular diseases.

3.   PM may directly impact the autonomous nervous system and as a result, cause cardiovascular diseases.
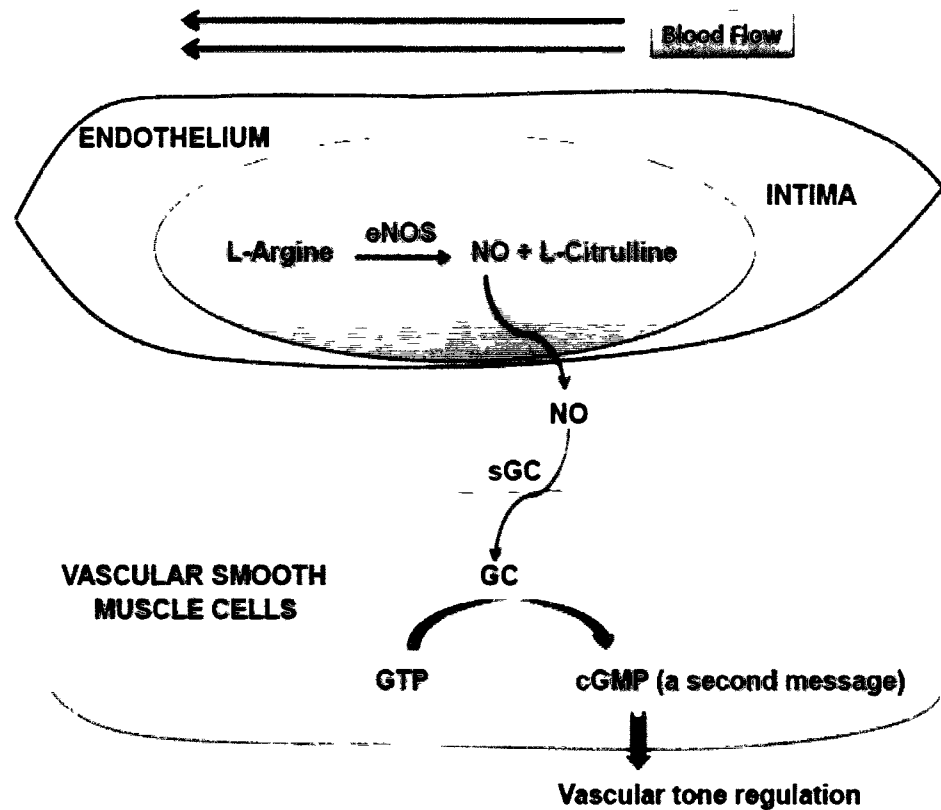
Figure 3. Nitric oxide biosynthesis.

The second mechanism listed above on the PM-induced endothelial dysfunction was the focus of this study. The related topics are marked by the shaded boxes in Figure 4. In the cardiovascular disease risk group, studies have shown that the endothelial dysfunction is usually caused by the increase of ROS, which can generate lipid peroxidation, oxidize NO and uncouple eNOS (Desjardins and Balligand 2006). Schneider demonstrated that endothelial dysfunction, including flow-medicated dilation (FMD) and small artery elasticity is associated with the depletion of NO bioavailability as well (Schneider et al. 2008). Furthermore, the generated lipid peroxidation can directly interact with NO (Rudolph and Freeman 2009; O'Donnell and Freeman 2001) or impair the eNOS activity to further alter NO production (Samii 2003; Rajagopalan et al.

2005). Rajagopalan hypothesized that PM may follow the same pathways as those

demonstrated in the cardiovascular disease risk group to potentiate the cardiovascular

disease (Rajagopalan et al. 2005). However, very limited studies have been conducted to

confirm the hypothesis that ambient PM and its components do affect NO bioavailability.

Thus, the hypothesis motivates this study to place its focus on the pathways of PM

derived NO bioavailability.
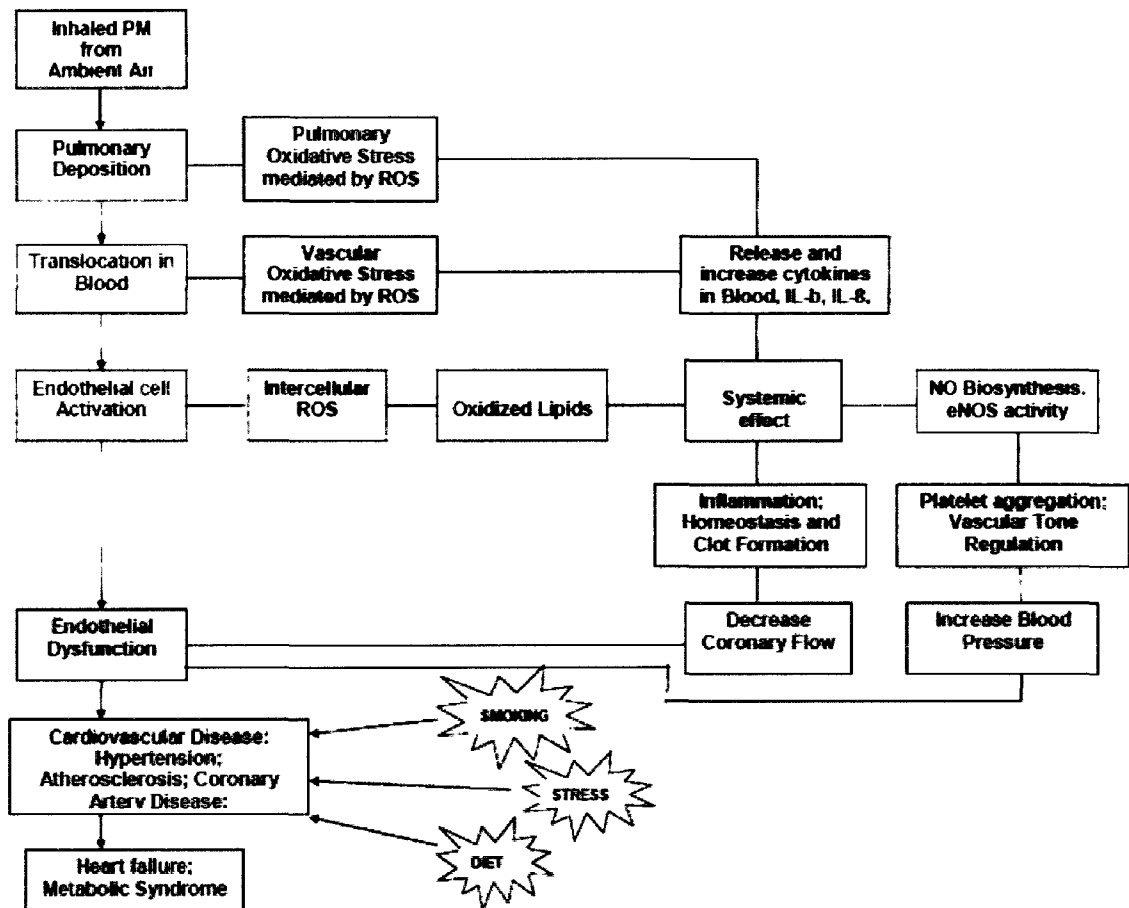
Figure 4. Hypothetical pathways of PM into cardiovascular system. (Delfino et al. 2005; Simkhovich et al. 2008) * represents the related reference in the hypothesis.

SPECIFIC AIMS

The central hypothesis of this study is that through ROS and lipid peroxidation,

PAHs affected NOS, which in turn altered the biosynthesis process of NO (Figure 5).

The investigated pathways were summarized as follows. PAHs activated endothelial

cells, therefore increased intracellular ROS generation, which in turn oxidized lipids in

the cell membranes and inhibitted eNOS activity.
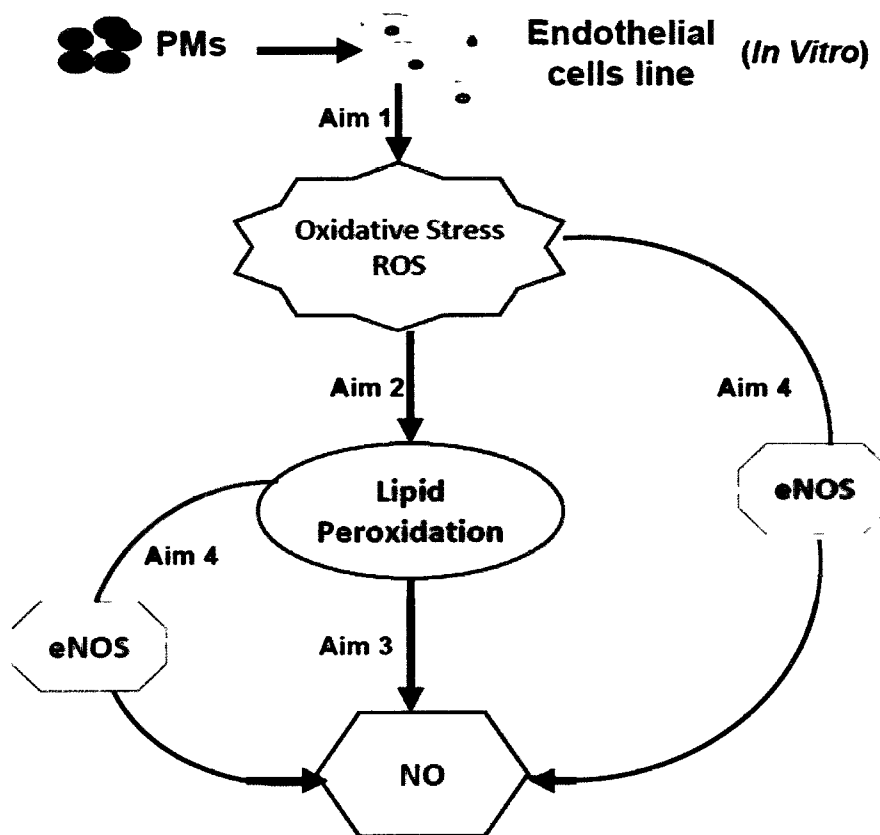
Figure 5. Possible PM-mediated Pathways on lipid peroxidation and NO bioavailability

To address the proposed hypothesis, specific aims were to:

- Confirm that PM exposure increased the generation of ROS, which resulted in oxidative stress in endothelial cells.

- Access whether PAHs increase oxidative stress in endothelial cells.

- Determine alteration of lipid profiling induced by lipid peroxidation.

- Assess whether PM and/or PAHs affect NO bioavailability by determining NO concentration and eNOS activity

- Determine whether PM and/or PAHs inhibit eNOS catalytic activity in relation to lipid peroxidation.

SIGNIFICANCE

The findings from this study increased the understanding of how PAHs alter endothelial cell function and damage via the pathway mechanism by which cells undergo oxidative stress. The results of this study would provide new insights into the mechanisms related to PM induced cardiovascular diseases, particularly atherosclerosis. On health perspectives, the finding of this study would link air pollution to cardiovascular diseases in biochemical terms, which pave a way to further investigate the adverse effects of PM exposure. Such knowledge will increase awareness of health risks of ambient particles and as a result, make us more sensitive to the control of the emissions and compositions of PM.

CHAPTER II

POLYCYCLIC AROMATIC HYDROCARBONS AS THE MAJOR COMPOENTN OF PARTICULATE MATTERS INDUCE OXIDATIVE EFFECTS TO ENDOTHELIAL CELLS *IN VITRO*

INTRODUCTION

Organic extracts of PM can produce superoxide and hydroxyl radical during incubation at 37 °C with or without biological activation system (Wells et al. 1997). PAHs in PM are the most abundant non-polar substances in the urban atmosphere and have become pollutants of serious concern. After absorption, PAHs are efficiently metabolized in many human tissues, especially in the vascular vessels. Alveolar capillary endothelium lies close to alveolar epithelium (Bai et al. 2001), thus the inhaled PAHs in PM may easily interact with vascular endothelium and blood by producing reactive oxygen and soluble materials.

Currently, there is no available data regarding PAHs toxicity on human coronary artery endothelial cells (HCAEC) in order to assess its role on PM-induced cardiovascular diseases. This study aimed to evaluate the oxidative stress generated in HCAEC induced by PAHs exposure. Specific aims include: 1) investigate cytotoxicity induced by PM to confirm its effects observed in the literature; 2) examine cytotoxicity and ROS generation in human endothelial cells induced by PM and PAH exposure.

EXPERIMENTAL PROCEDURES

Materials

A23187 calcium ionophore was obtained from Sigma-Aldrich (St.Louis, MO). Albumin standard was obtained from Pierce (Rockland, IL). Apocynin was obtained from Fisher Scientific (Pittsburgh, PA). β-Nicotinamide adenine dinucleotide phosphate, reduced tetra (cyclohexylammonium) salt was obtained from Sigma-Aldrich (St.Louis, MO). 99.8% chloroform was obtained from Acros (Thermo). Cell culture flasks and dishes were obtained from Corning (Corning, NY). Cell lysis buffer was obtained from New England Biolabs (Beverly, MA) and supplied as 10X cell lysis buffer. 8 chamber tissue culture treated glass slide was obtained from BD Falcon (Bedford, MA). Comassie protein assay kit was obtained from Pierce (Thermo, Rockford, IL). Disel particulate matter was obtained from National Institute of Standards and Technology (NIST, Geithersburg, MD). Dimethyl sulfoxide (DMSO) was obtained from Sigma. Ethylenediaminetetraacetic acid (EDTA) was obtained from Sigma. Ethylene glycol-bis(2-aminoethylether)-N,N,N',N'-tetraacetic acid (EGTA) was obtained from Sigma. Glass tubes, borosilicate (16x100mm), were obtained from Fisher. Human coronary artery endothelial cells (HCAEC) were purchased from Cell Applications, Inc. (San Diego, CA) and grown in culture at 37°C and 5% CO2 cells were grown in Medoendo Eell Growth Media. Hank's balanced salt solution, calcium- and magnesium-free (HBSS) was obtained from Mediatech Cellgro (VA).30% H_2O_2 was obtained from Fisher Scientific. Homogenizer was obtained from Fisher Scientific. H2DFFDA was obtained from Invitrogen. Isopore membrane filters, 3.0μm TSTP and 1.2 μm RTTP, were obtained from Millipore (Billerica, MA). 8-Isoprostane Express EIA Kit (Catalog #516360) was obtained from Cayman Chemical

(Ann Arbor, MI). Lactate dehydrogenase (LDH) Kit (Cat.# 04744926001) was obtained from Roche. β-Nicotinamide adenine dinucleotide phosphate, reduced tetra(cyclohexylammonium) salt (NADPH) was obtained from Sigma. 99% methyl alcohol was obtained from Acros (Thermo). Mounting medium for fluorescence with DAPI was obtained from Vector (Burlingame, CA). Nω-Nitro-L-arginine methyl ester hydrochloride (L-NAME) was obtained from Sigma-Aldrich (St.Louis, MO). Polypropylene centrifuge tubes (15ml) were obtained from Corning Inc. (Corning, NY). Polycyclic aromatic hydrocarbons were obtained from Restek (Bellefonte, PA). Sodium dodecylsulfate (SDS) was obtained from American Bioanalytical. Sodium hydroxide (NaOH), 10N solution, 30% w/w, was obtained by Fisher Scientific. Thiobarbituric Acid Reactive Substances (TBARS) Assay Kit (Cat.# 0801192) was obtained from ZeptoMetrix Corporation (Buffalo, NY). Total Nitric Oxide Assay Kit (Lot # KG134678) was obtained from Thermo Scientific (Rockford, IL). Triton-X100 was obtained from Fisher Scientific. Trypan blue solution (0.4%) was obtained from Sigma-Aldrich (St.Louis, MO). Phosphate buffered saline 10X was obtained from Fisher Scientific. PTFE cap and target vials were obtained from Fisher scientific. All aqueous solutions and reagents were prepared in deionized distilled water using ELGA Purelab system from SIEMIENS.

Cell Culture and Preparation

Endothelial cells are economical alternative, suitable for studies of endothelial functional and endothelial metabolism. Changes in structure and function of these cells have been linked to vascular diseases such as atherosclerosis, and hypertension. Human

coronary artery endothelial cells (HCAEC) used in this study was isolated from normal

human coronary arteries from Cell Application (San Diego, CA). HCAEC were grown in

Mesoendo Cell Growth Medium that is fully supplemented with fetal bovine serum,

growth factors, trace elements and antibiotics. The cells in culture flasks were placed in

an incubator at 37 °C with a humidified atmosphere of 5 % CO_2. Cells were preserved

and stored with liquid nitrogen in a cryosystem (Cryogenic locator, Thermo).

HCAEC was cultured for treatment when cells are about 80-90% confluent. Cells

were used for all experiments on the passages 5 to 15. Active proliferation cells were

exposed to fine particle or PAHs solutions prepared as described below. After exposure,

cells were harvested from cultured flask. This involves removal of media from flask, a

rinse with Hank's Balanced Salt Solution 1X, trysin EDTA 1X 0.25 % trypsin/2.21 mM

EDTA in HBSS addition and Mesoendo Cell Growth Medium addition. HCAEC

preparation prior to bioassays involves centrifugation at 1092 rpm (200g), removal

supernatant, followed by HBSS wash twice. Cell count was performed using a

hemacytometer.

Particulate Matter Preparation

Diesel particulate matter (DPM), 2975-Industrial forklift, was obtained from

National Institute of Standards and Technology (NIST, Geithersburg, MD). The

certificate of analysis of DPM provided concentrations of PAH (i.e. phenanthrene,

fluoranthene), the percent of extractable mass, and particle size (Appendix A, Appendix

B, Appendix C).

Since the average particulate size of the DPM was less than the inhalation average particulate size established by the American Conference of Government Industrial Hygienists (ACGIH), proper inhalation/respiratory protection was employed according to the Occupational Safety and Health Administration (OSHA) Respiratory Protection Standards 29 CFR Part 1910.134 (Protection. Regulations (Standards-29 CFR)).

Fine particle were isolated from diesel particulate matter using a multistep filtration process to remove particles and agglomerates larger than 3 μm. Briefly, diesel particulate matter was weighted and suspended in HBSS to reach a concentration of 15 mg/L. The particulate matter was vigorously stirred; the suspension was sonicated in a water bath sonication for 15 minutes. The homogenous suspension was filtered through a 3-μm pore polycarbonate filter. This process moved particles and agglomerates > 3 μm in diameter. The filtrate was filtered through 1.2 μm pore polycarbonate filter once again, which removed particles with diameters > 1.2 μm. The final filtrate containing fine particle was used to treat cells. The particle solution was prepared and diluted immediately before cell exposure, and diluted as required.

Assessment of Particle Size Distribution

Size distribution of particles was measured by Zetasizer (Nano-series, Malvern Instruments). The zetasizer performs size measurements by first measuring the Brownian motion of the particles in a sample using Dynamic Light Scattering (DLS), Bronian motion is defined as the random movement of particles in a liquid due to the bombardment by the molecules that surround them. And then relate this to the size of the

particle by illuminating the particles with a laser and analyzing the intensity fluctuations in the scattered light.

Fine particle were prepared and diluted as described above. Size distribution was displayed by intensity graph as a higtogram, with logarithmic X-axis and linear Y-axis settings.

Polycyclic Aromatic Hydrocarbons Preparation

EPA method 8310 PAH Mixture was obtained from Restek Corporation. Acetonitrile with composition of 99.1 % was used as solvent. Certificate of analysis provided PAH compound and concentration (Appendix D). Ultrasonication was used to remove air bubbles or to breakup agglomerates before loading 1 ml of the sample into disposable polystyrene cuvettes. The PAH solution was prepared and diluted immediately before cell exposure, and diluted as required. Cells were exposed to PAH with variable factors of exposure, including the concentration and the duration time of exposure.

Personal protection was taken followed the safety data sheet to prevent exposure. Respiratory mask, safety glasses, and gloves were used to protect respiration, eyes and skin when handling PAHs (RESTEK 2010).

Assessment of Polycyclic Aromatic Hydrocarbons Cytotoxicity

Lactate dehydrogenase (LDH), a stable enzyme located in the cytosal, was rapidly released into the surrounding culture medium upon cell membrane damage or lysis, processes that occur during both apoptosis and necrosis. The LDH activity was

determined in an enzymatic test, firstly LDH catalyzes the reduction of NAD^+ to

$NADH/H^+$ by oxidation of lactate to pyruvate. In the second step, diaphorase transfers the

new-formed NADH and H^+ to catalyze the reduction of a tetrazolium salt (INT) to

highly-colored formazan which absorbs strongly at 492 nm.

The Cytotoxicity Detection Kit (Roche Applied Sciences, Germany) was used for

quantitating cytotoxicity of PAH to cells. Based on the preliminary study on

determination of the optimal cell concentration, a density of 2.5×10^4 cells/well was

decided to seed in a 96-well plate with 100 µl of culture medium per well. The procedure

was followed according to the manufacturer's instructions. The cytotoxicity was

calculated and described as percentage.

Evaluation of Cell Morphology

Cell morphology was viewed by Nikon Light microscopy TS 100. The bright

field images were captured by a Cool Snap EZ camera.

The flow cytometry was also employed to analyze many properties of many cells

and to study cell morphology with a number of detectors, which were aimed at the point

where the stream passes through the light beam, one in line with the light beam (Forward

Scatter or FSC) and several perpendicular to it (Side Scatter or SSC) and one or more

fluorescent detectors. The intensity of FSC signal has been attributed to cell size,

refractive index or membrane permeability. The intensity of SSC signal was proportional

to the amount of cytosolic structure in the cell, such as granules and cell inclusions,

where laser light that was scattered at 90 degrees to the axis of the laser path is detected

in the side scatter channel. Since FSC associated with the cell size and SSC depended on

the inner complexity of the particle, a correlated measurement between them can allow for differentiation of cell types in a heterogenous cell population.

Evaluation of Cell Viability

HCAEC were cultured as previously mentioned, and were harvested from the cultured flask, washed, and then resuspended. Cell viability was assessed by staining with 0.02 % trypan blue in HBSS, and cell counts of 100 cells were performed using a hemacytometer after 2 minutes with a Nikon Eclipse TS 100 light microscope.

Detection of Reactive Oxygen Species

ROS detection was performed using the Image-iT LIVE Green Oxygen Species Detection Kit (Molecular Probes). The assay is based on 5-(and-6)-carboxy-2', 7'-dichlorodihydrofluorescein diacetate (carboxy-H_2DCFDA), a cell permeable, non-polar, H_2O_2-sensitive fluorogenic probe for ROS in live cells. Oxidation of this probe can be detected by monitoring the increase in fluorescence with a fluorescence microscope, using excitation sources and filters appropriate for fluorescien (FITC) (Oksvold et al. 2002; Konorev et al. 2000).

The procedures of labeling with Carboxy-H_2DCFDA are as follows:

Prepare a 10 mM carboxy-H_2DCFDA stock solution by adding 50 µL of DMSO to one vial of carboxy-H_2DCFDA to make a 10 mM stock solution. Vortex the vial until the powder is completely dissolved. Then prepare 25 µM carboxy-H_2DCFDA working solution by adding 5.0 µL of the 10 mM carboxy-H_2DCFDA stock solution to 2.0 ml of warm HBSS buffer. After that, cells are washed gently with warm HBSS followed by

labeling cells. In order to do so, apply a sufficient amount of the 25 μM carboxy-

H_2DCFDA working solution to cover the cells adhering to the cover-slip. Incubate for 30

minutes at 37 °C, protected from light. Again, cells are washed gently twice in warm

HBSS. The final step is to mount cells in warm buffer and image immediately by

mounting medium, using a DAPI filter set and neutral density filter(s) to assist with

locating the cells on the cover-slip, followed by a fluorescein filter set for imaging.

Quantification of ROS

2', 7'- difluorodihydrofluorescein (C13293, Invitrogen), an oxidant by-product of

5-(and-6)-carboxy-2', 7'- difluorodihydrofluorescein diacetate (carboxy-H_2DFFDA), was

used to assess the ROS generation in HCAEC. Cells were incubated with H_2DFFDA (10^{-5} M) for 0.5 hour at 37 ° C and washed twice with Hank's Buffered Salt Solution.

HCAEC were after cultured in the presence or absence of fine particles or PAHs for 1

hour. H_2O_2 (100 μM) was used as a positive control to induce oxidative stress. After an

extensive wash, fluorescence of fine particle treated cells was evaluated by flow

cytometry (FASCCalibur, Becton Dickinson) at Eastern Virginia Medical School

(Norfolk, VA); fluorescence of PAHs treated cells was evaluated by flow cytometry

(FASCAria, Becton Dickinson) at Bioelectric Center, Old Dominion University (Norfolk,

VA). The mean fluoresce intensity was calculated by multiplying the number of

fluorescent cells by the mean of the intensity presented by the Flow-Jo software used for

the analysis.

Statistical Analysis

Statistical analysis was performed using Sigma-Plot software. All experiments were carried out in triplicate, and results were expressed as means ± standard error of the mean (SEM). Comparisons involving three or more groups were evaluated using one-way ANOVA and an appropriate *post hoc* comparison. Instances involving only two comparisons were evaluated with a Student's *t*-test. Differences among means were considered statistically significant by the criterion of probability P value ≤ 0.05.

RESULTS

Size distribution of PM

In the initial phase of investigation, the size distribution of the fine particles after filtration has been analyzed by the Zetasizer Nano series from Malvern. Size distribution of fine particles is showed in Figure 6. After filtration with 3.0 μm pore size filter, particles with larger size in DPM were removed. In the filtrate, 82.6% of particles had diameters at 220.8 nm on average, 17.4% of particles had diameters at 4827 nm. After filtration with 1.2 μm pore size filter, 94% of particles were at the diameter of 262.3 nm, and 6% of particles were at 4546 nm. From the correlation graph, we conclued that this results met the quality criteria. The prepared fine particles at this step were used in the following studies.

The filtrated fine particles were smaller in mass than DPM; they also had larger surface area to contact with cells. In addition, their numbers are higher as compared to other particles. Thus, fine particles had the potential to enter blood stream and affect the endothelium directly.
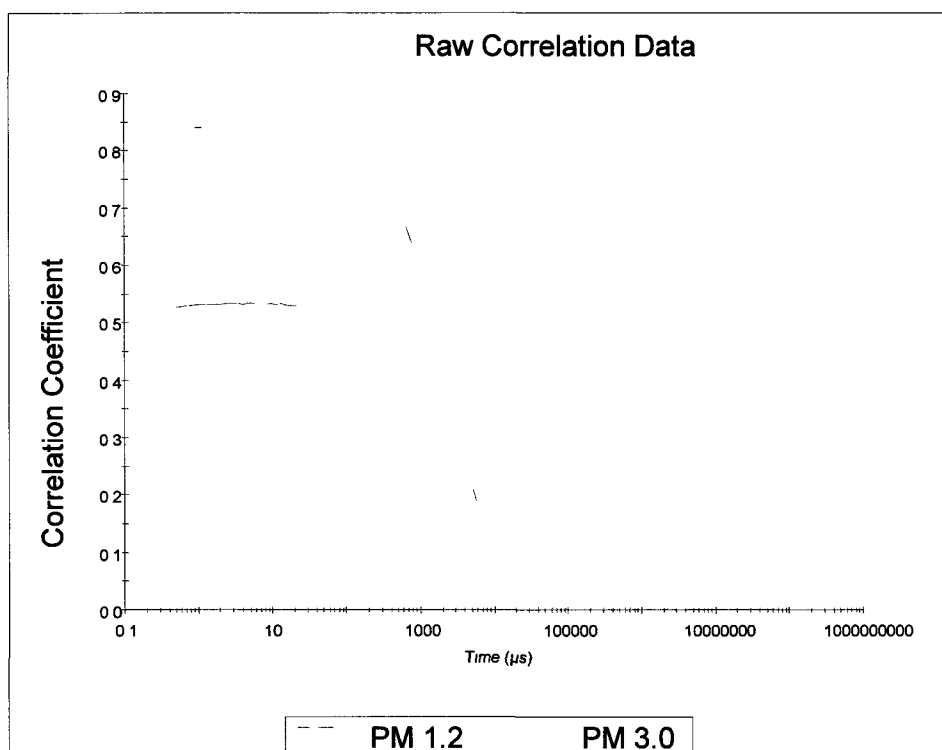
A
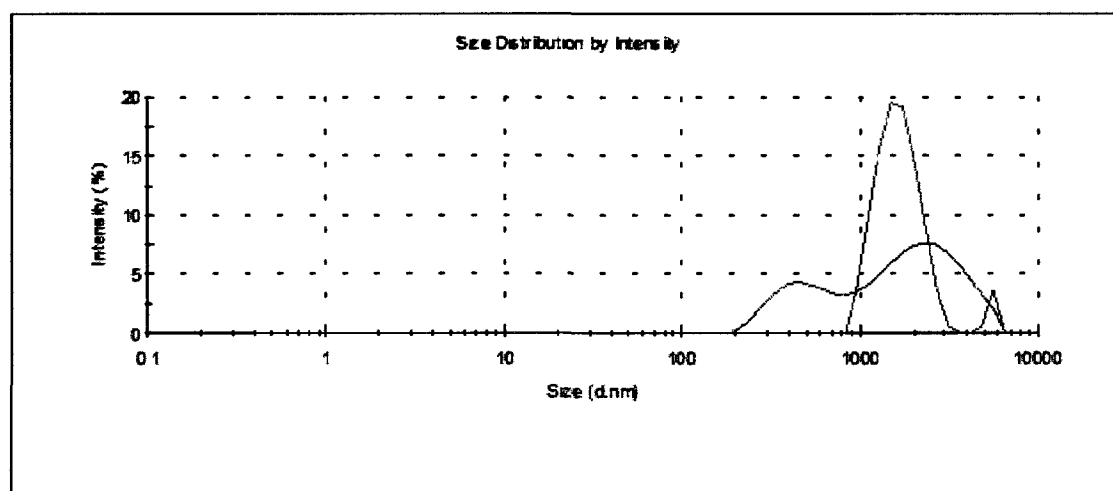
B

Figure 6. PM size distribution by Zetasizer Nano Series. PM size correlation data (*A*), size distribution by intensity *(B)*. Green line and red line represent particle size distribution after filtration with 3.0 μm pore size filter and with 1.2 μm pore size filter, respectively.

Cytotoxicity of PM

Cell morphology changed after PM exposure

Figure 7 showed control cells, cells treated with PM, PM only groups. Cell size was measured and showed in Table 1. After PM treatment, size of HCAEC decreased 32.5 % compared to control, illustrating that cell shrinkage took place after PM exposure. Results were presented as mean ± SEM of 10 independent experiments and were expressed as μm, $p < 0.05$ are considered as significant differences.

Cells were washed twice with HBSS after exposure, and then images were taken under bright field microscopy. HCAEC morphology had obviously changes after PM treatment (Figure 7). Cell shape turned to be elliptical. Particles were observed to pass through the cells membrane and enter the cells indicated as the arrows in Figure 7B. Decreases in cell size were also noticed after PM exposure. It is likely that PM comprised integrity of cell membrane that allows cytosol and intracellular fluid leaked to the surroundings.

Table 1. HACEC size measurements. Sample number counted in each group is 10; * indicates P<0.0001 compared with cells only

	Cells Only	PM treated Cells	PM only
Cells sizes, μm	30.8 ± 1.48	20.8 ± 1.04 *	3.0
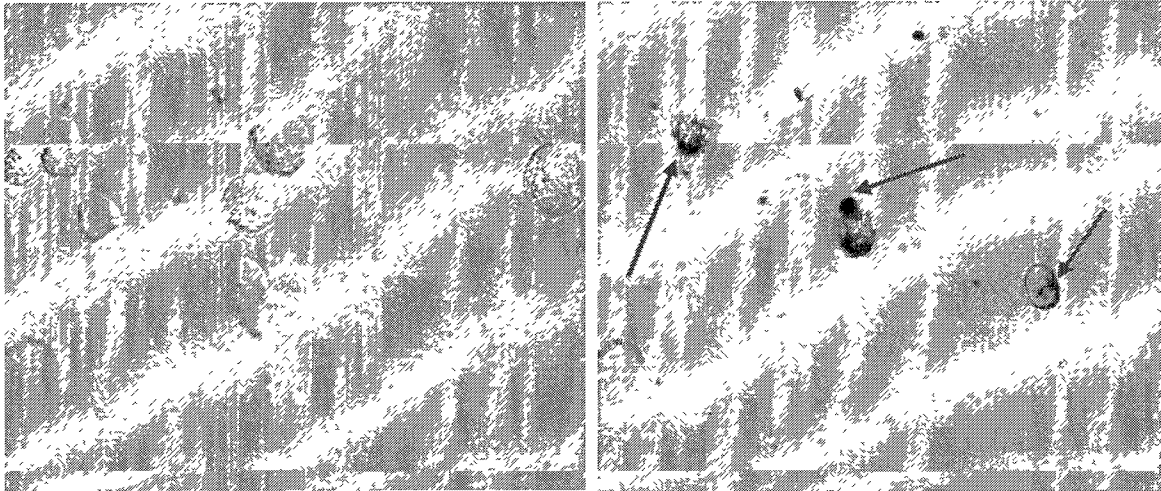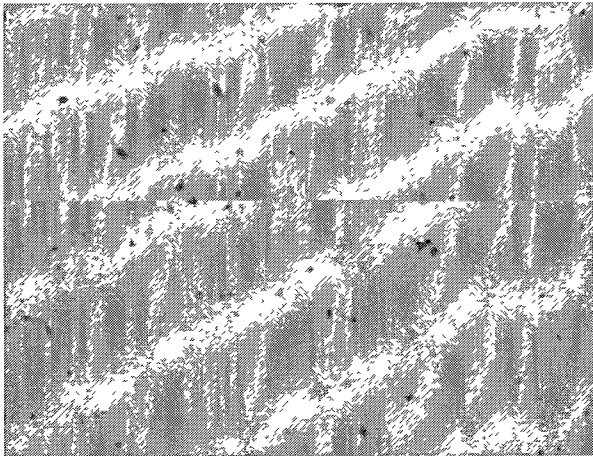
Figure 7. Cell morphology changed after PM treatment (400X). Cells Only (*A*), 1 mg/L PM for 1.0 hour treatment (*B*), PM only (*C*). Cell images were token with a Nikon diaphot light microscopy.

Cell viability changed after PM exposure

After PM exposure, cell populations had an obvious shift from the histograms in Figure 8 from the flow cytometer results, the whole group had the trend to move to the upper left. Also cell shrinkage took place due to the stimulation of PM.

FSC readings decreased, indicating that cell size was reduced. The increased reading of SSC showed that the internal structure of HCAEC altered and the granularity on cell membrane increased. Cell viability decreased since more debris had been noticed after PM exposure as well as the H_2O_2 treatments as a positive control. These observations confirmed the results that cell shrinkage took place after PM exposure, the shape of nucleus were changed, cell membrane was damaged and resulted in membrane roughness due to the increasing amount of cytoplasm granules.

After PM exposure, cell viability decreased in both 0.5 hour and 1.0 hour incubation groups. More dead cells were dyed with trypan blue in PM treated groups, revealing that cell membrane was injured. HCAEC viability of 0.5 and 1.0 hour PM exposure decreased 1% and 5%, respectively, compared to control in Figure 9. HCAEC treated with H_2O_2 decreased 18.7%. We expected to see harsh effects to cell viability after PM exposure; however, the reading has no significant decrease, nor time- dependent pattern.

Control

H₂O₂ treated Cells

PM treated 0.5 hour Cells.

PM treated 1.0 hour Cells
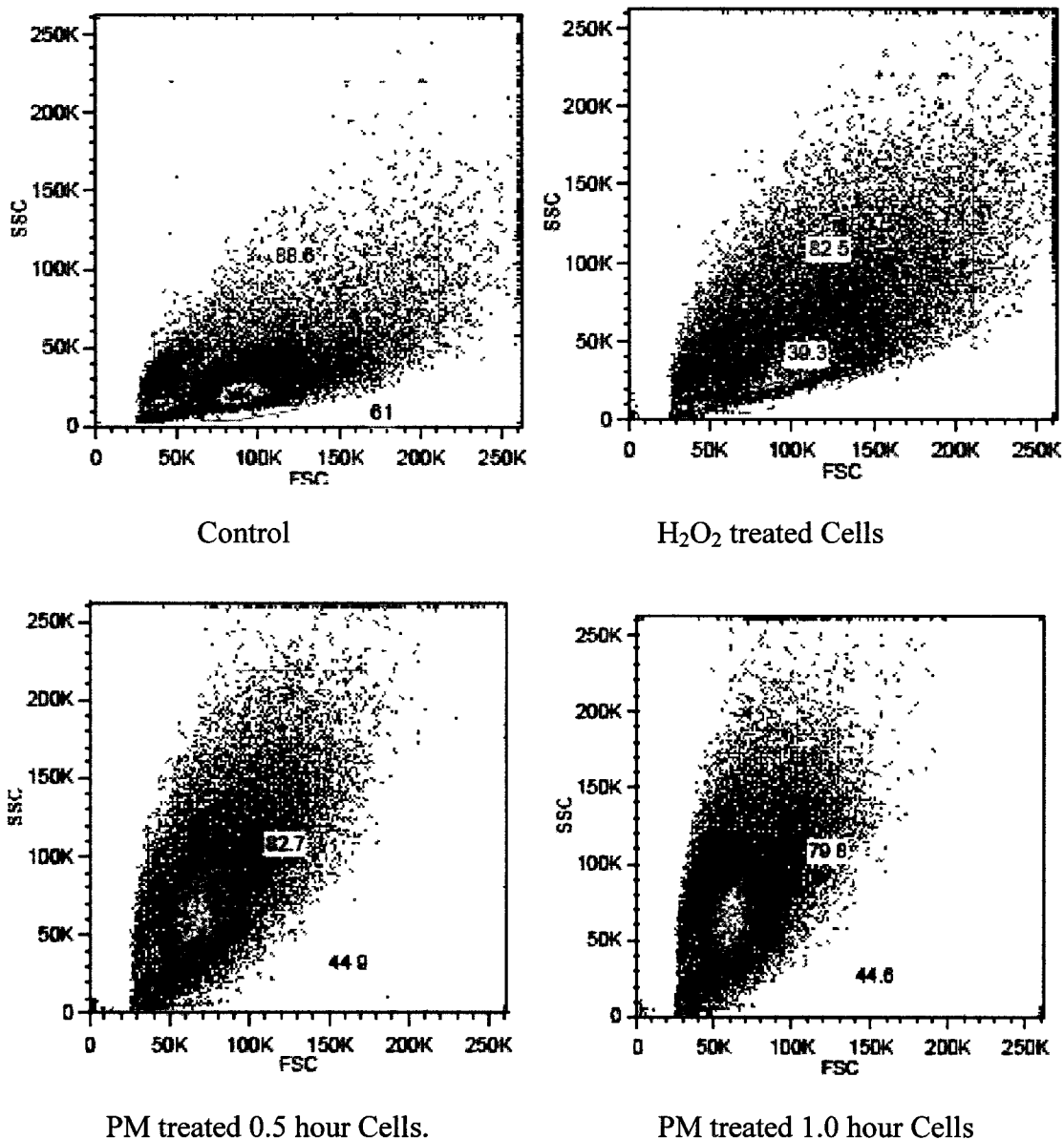
Figure 8. Histograms of PM treated cells. HCAEC were treated with 1 mg/L PM for 0.5 and 1.0 hour, following with H₂DFFDA dye. 100 μM/ml H₂O₂ were introduced to cells as positive control. Cell population was displayed and distributed with a flow cytometer. Cells gated in rectangle with percentage were counted as total cells. Cells gated in elliptical with percentage of total cells were counted for viability analysis.
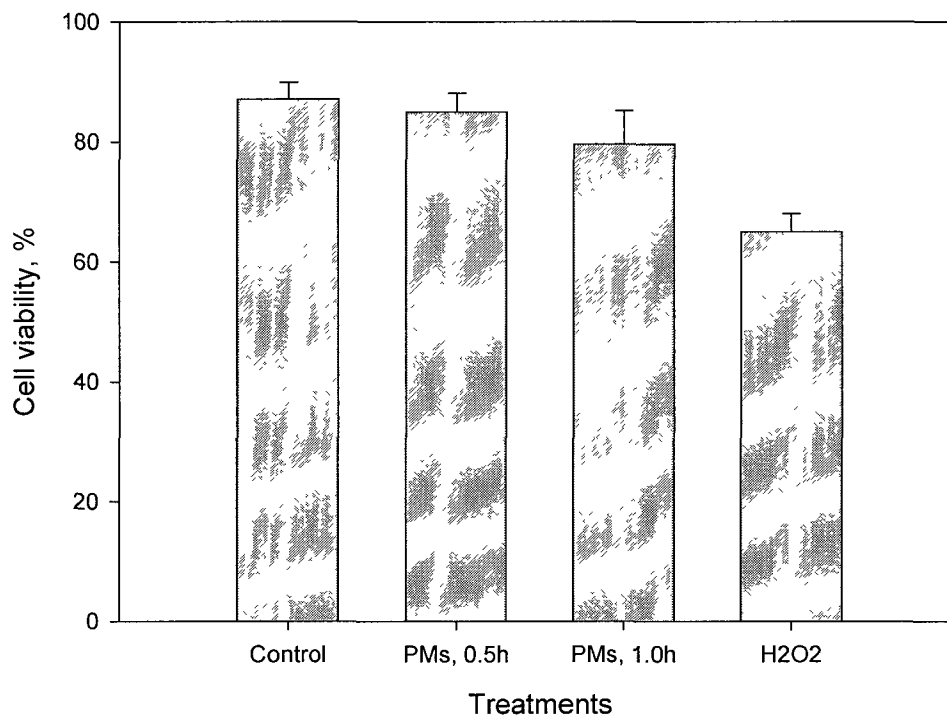
Figure 9. Cell viability after PM exposure. HCAEC were incubated with 1 mg/L PM for 0.5 and 1.0 hour. 100 μM/ml H_2O_2 were introduced to cells for 0.5 hour as positive control.

ROS generation by PM treated HCAEC

Fluorescent dye DCFDA was detected in the cells exposed to PM at

concentrations of 0.1, 1 and 10 mg/ml. The fluorescent intensity from those treated cells

by PM was significantly increased as compared to the control (Figure 10). Interesting,

the cells treated by PM at 1 mg/ml seemly had strong fluorescent expression than those

treated by 10 mg/ml PM. The higher concentration of PM at the concentration of 10

mg/ml may overshadow the fluorescence intensity. The flow cytometry method

confirmed that fluorescence from the dye DFFDA was generated in the cells treated by

PM (Figure 11). PM induced ROS generation in HCAEC after 1.0 hour exposure, while

PM has minimal effects on ROS generation in HCAEC after 0.5 hour exposure (Table 2).

No significant differences existed between PM treated groups and the control (p value of

PM 0.5 hour treatment is 0.210; p value of PM 1.0 hour treatment is 0.031). The

inconsistent results may be caused by the attachment of the fine particles on cell

membrane and/or translocation of fine particles into the cells blocked fluorescence, and

subsequently altered the degrees of fluorescent intensity detected by a flow cytometer.

Control   100 µg/ml

1 mg/ml   10 mg/ml
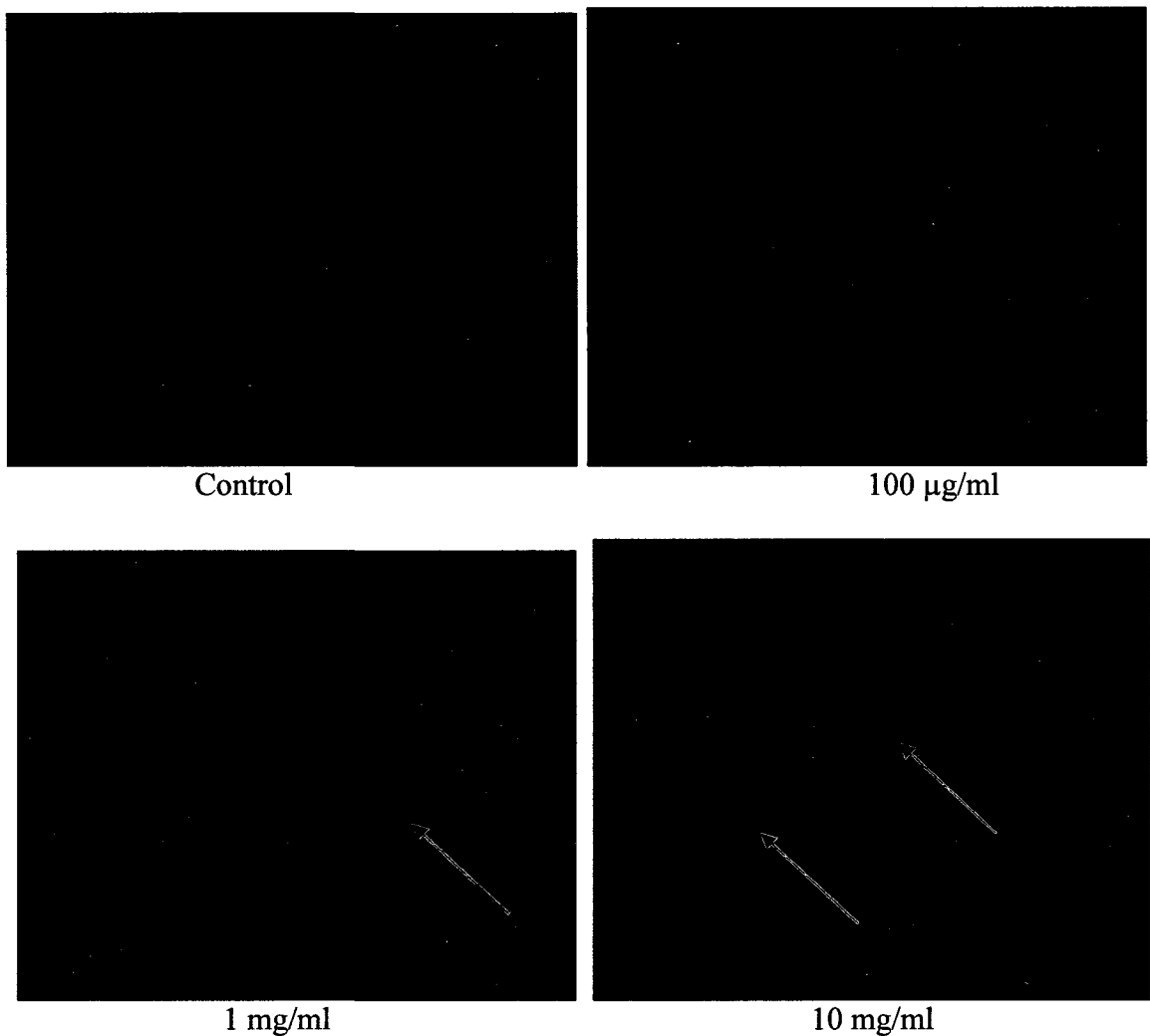
Figure 10. Effects of PM on ROS generation. HCAEC was exposed to 0.1, 1 and 10 mg/ml PM concentrations for 12 hours following with the incubation with Carboxy-H_2DCFDA. (400x)

PM 0.5 hour
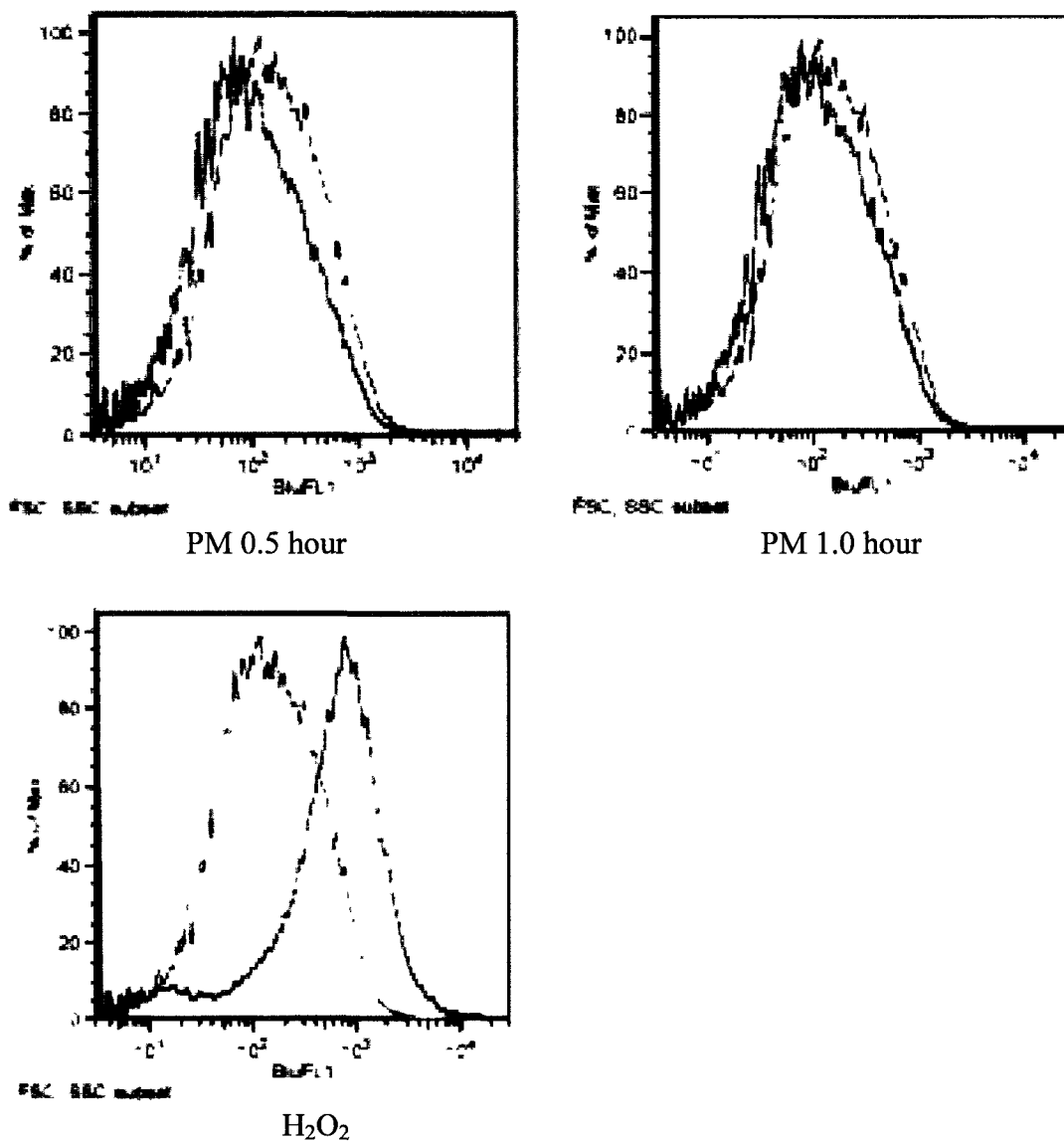
PM 1.0 hour

H_2O_2

Figure 11. Overlapped ROS generation after PM treatment. HCAEC were incubated with 1 mg/L PM for 0.5 and 1.0 hour following with the incubation with H_2DFFDA. 100 µM/ml H_2O_2 were introduced to cells for 0.5 hour as positive control. Red line represented control cells, blue line represented cells treated with PM for 0.5 hour, PM for 1.0 hour and H_2O_2 for 0.5 hour, respectively.

Table 2. Fluorescence of PM treated groups

Treatment	Control	PM, 0.5 hour	PM, 1.0 hour	H_2O_2
Fluorescence Units Mean	660	639	723	845

Cytotoxicity of PAHs exposure

Cell morphology and variability change after PAHs exposure

Figure 13 shows cell treated with PAHs were shrunk and detected from the culture flask. After exposure to PAHs for 0.5 h, cell morphology was noticeably changed, granularity increased, shrinkage was observed, and viability decreased. A group of particles were noticeably appeared at the left of the cells in the PAHs treated groups, which were PAHs after comparing with the histogram result of the cell-free PAHs.

PAHs decreased viability of endothelial cells in a concentration-dependent manner. Since 3 hour exposure of PAHs decreased cell viability significantly at the concentration higher than10 µg/ml, and has more harsh effects than 1 hour. Thus, the concentration of PAHs with no more than 15 µg/ml, has been chosen in the following studies.

PAHs concentrations at < 7.5 µg/ml did not alter viability of endothelial cells after incubation for one and three hours. At the concentration of 10µg/ml, PAHs started causing decreased cellular viability in three-hour contact. The degree of the cytotoxicity continues to increase as the increase in PAH concentrations. After three hours exposure, significant differences were observed from PAHs 10, 15 and 25 µg/ml groups in comparison with control, p values were 0.0006, 0.0002 and 5.306E-20, respectively. That demonstrates the effect was in a dose-depended fashion

LDH is a stable enzyme located in the cytosal, which rapidly release into the surrounding culture medium upon cell membrane damage or lysis, this processes occur during both apoptosis and necrosis. This method indicated that integrity of cellular membrane was comprised by PAHs exposure to allow cytosol to release from the inside cells to the surrounding culture medium At the same time, the LDH assay showed that PAHs caused cytotoxicity to HCAEC.

Control   H₂O₂ exposure

1 μg/ml of PAHs 5 μg/ml of PAHs 12 μg/ml of PAHs
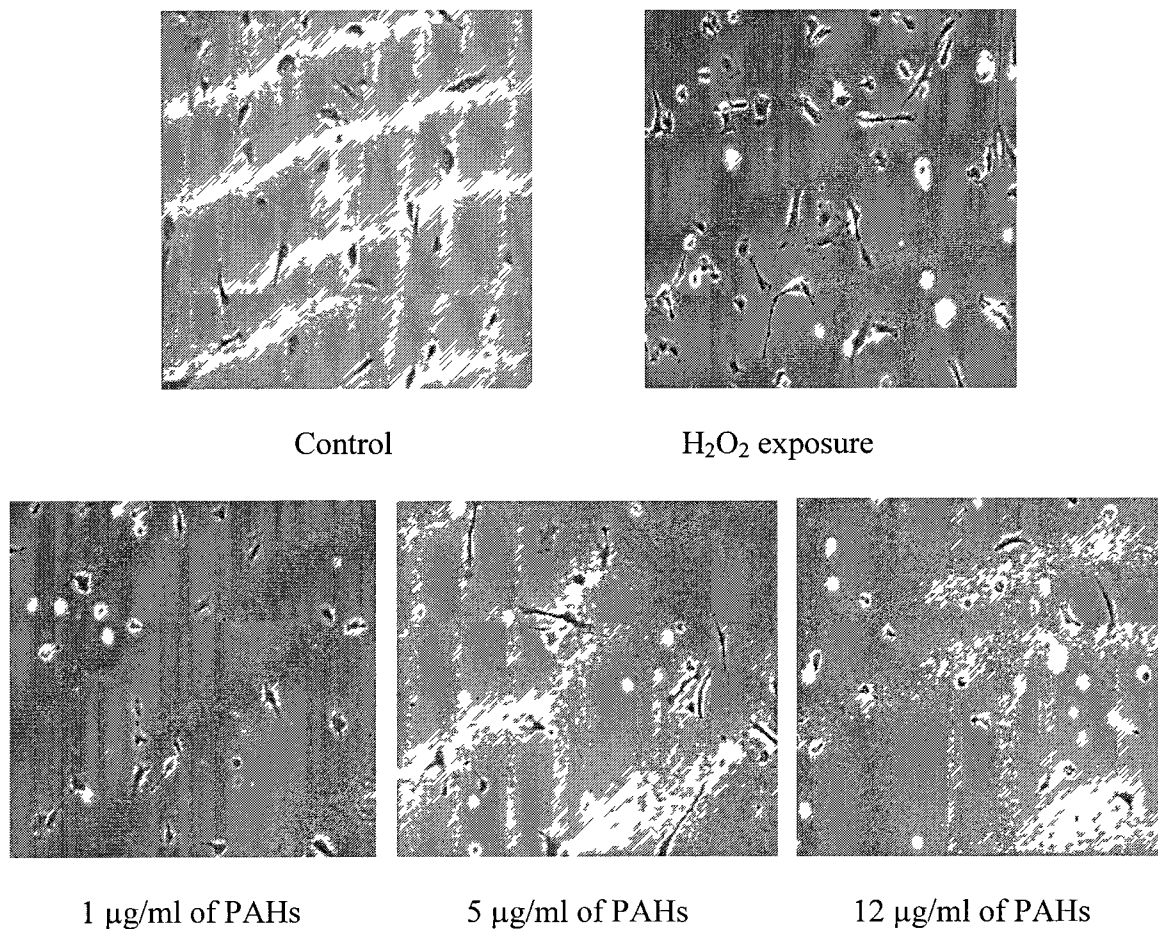
Figure 12. Cell morphology after PAHs exposure. Cells were treated with 0 (control), 1, 5 and 12 μg/ml of PAHs for 0.5 hour, respectively. Cells treated with H_2O_2 were used as positive control. Cell images were token under 100x
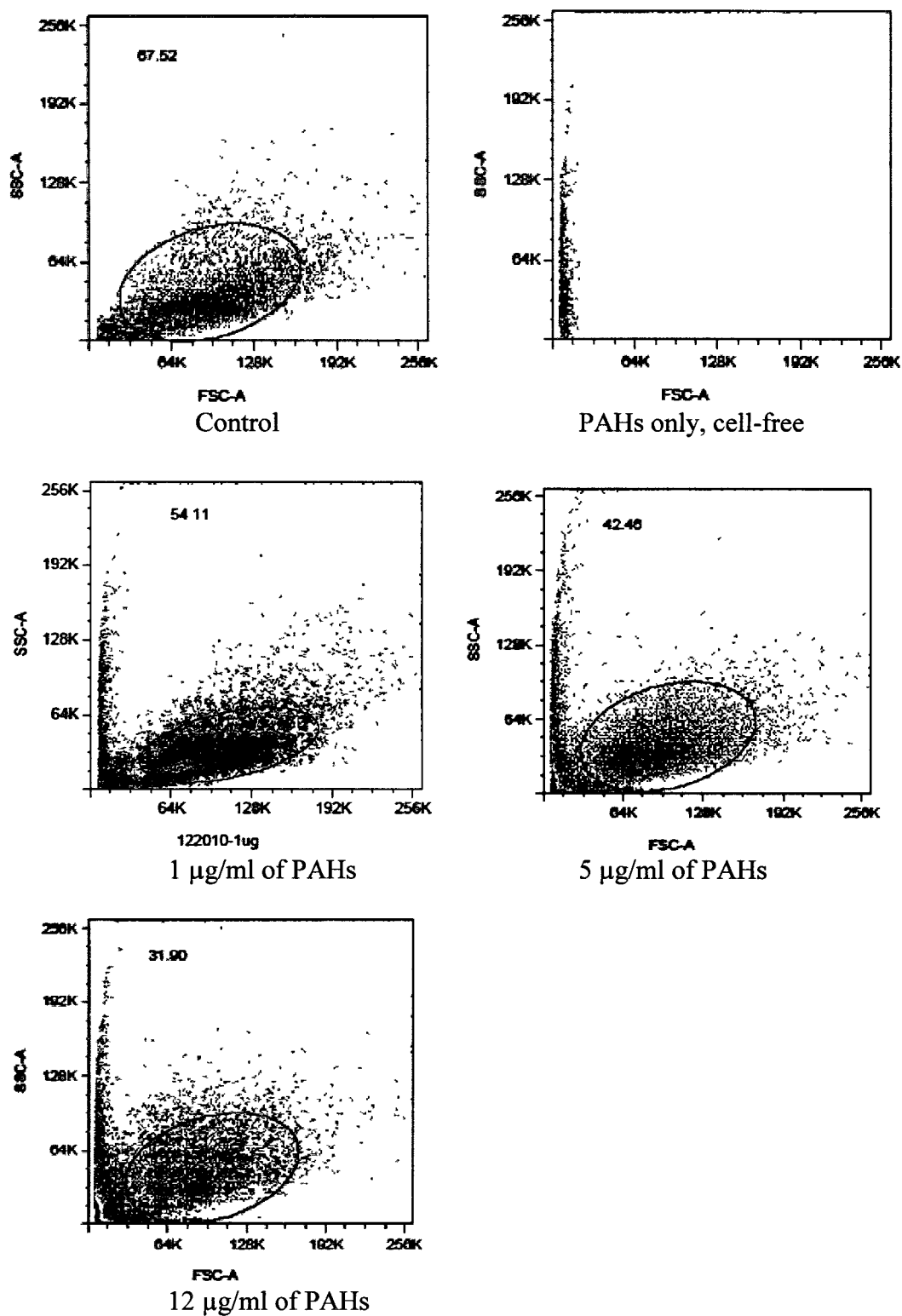
Figure 13. Histograms of PAHs treated groups. Cells were treated with 0 (control), 1, 5 and 12 µg/ml of PAHs for 0.5 hour, respectively. PAHs were detected in a cell-free condition as well.
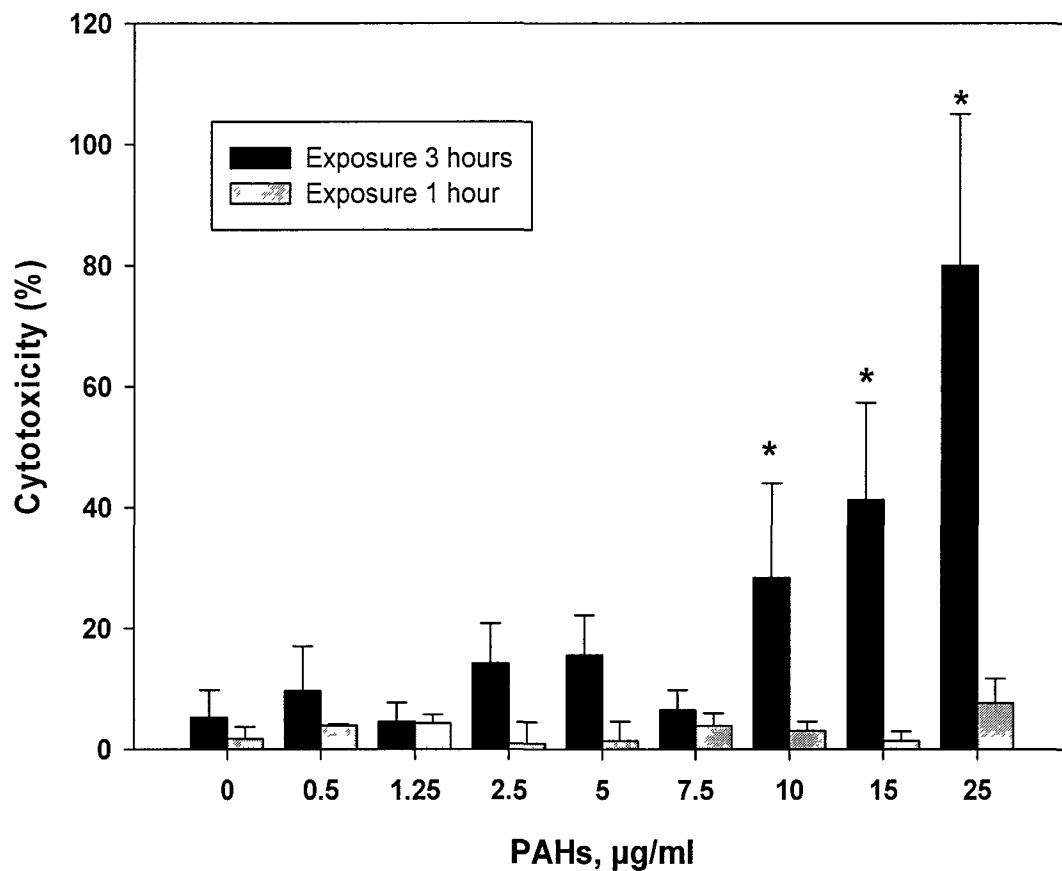
Figure 14. Cytoxicity of PAHs to HCAEC. HCAEC were incubated with different concentrations of PAHs, 0 (control), 0.5, 1.25, 2.5, 7.5, 10, 15, 25, and 50 μg/ml and cultured in HBSS at 37 °C for 1and 3hours. Lactate dehydrogenase method was used to measure the cytotoxicity of PAHs. LDH released into the media was assessed. Results are presented as mean ± SEM of three independent experiments and are expressed as percentage, $p < 0.05$ are considered as significant differences.

Vehicle effects on HCAEC

Cell morphology changed after CH₃CN exposure

99% pure acetonitrile were used as solvent in PAHs stock. After a series of dilution, the concentration of acetonitrile in the PAHs suspension for exposure was no more than 2%. Acetonitrile is colorless liquid that is mainly used as a polar aprotic solvent in purification of butadiene. Acetonitrile has only a modest toxicity in small doses (Wexler 2005). To ensure the observed cytotoxicity induced by PAHs instead solvent used to disovle PAHs, 2% CH₃CN was examined any toxic effects on HCAEC. Cell morphology has no significant differences after acetonitrile treatment (Figure 15). Cell distribution in vehicle treated group was the same with control from the histograms results in Figure 16.

ROS generation after CH₃CN exposure

No significant increase of ROS was observed from the results in Figure 17 (p value = 0.17). Therefore, the increase of ROS level and cell activation in the PAHs treated groups were not due to the effects of acetonitrile.

ROS generation in HCAEC after PAHs exposure

Microscopy photographs illustrated 1 and 5 µg/ml PAHs t induced the gerenation of ROS after 0.5 hour contact (Figure 18). Fluorescent cells were found in the PAHs treated groups, while absent in the control and vehicle treated group.
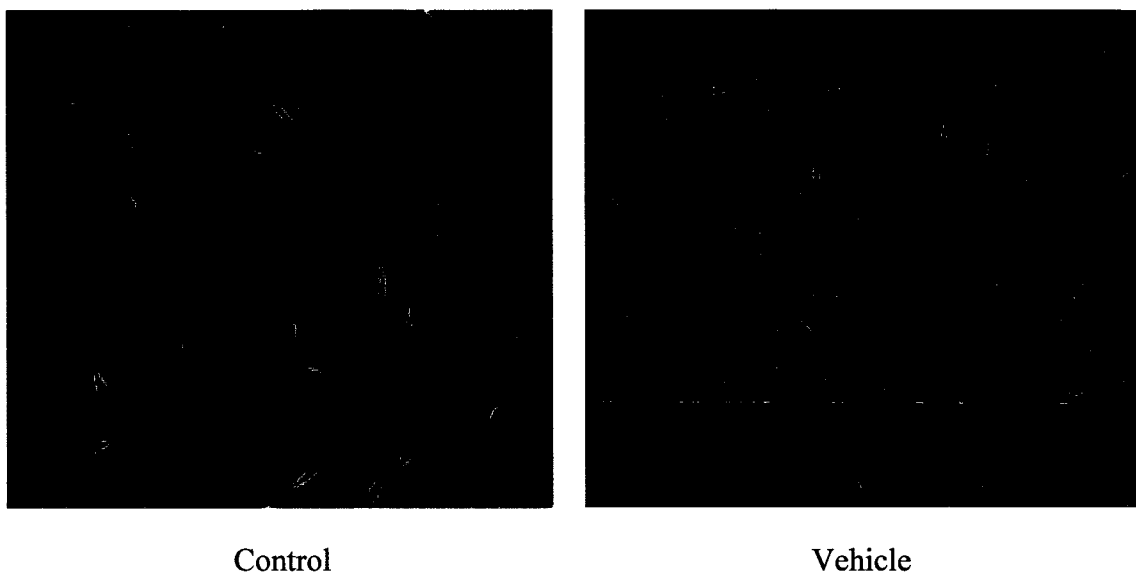
Control   Vehicle

Figure 15. Cell morphology after vehicle treatment. Cells were treated with 0 (control), 2% CH3CN for 0.5 hour, respectively. Cell images were token under 100x.

Control Group   Vehicle Group
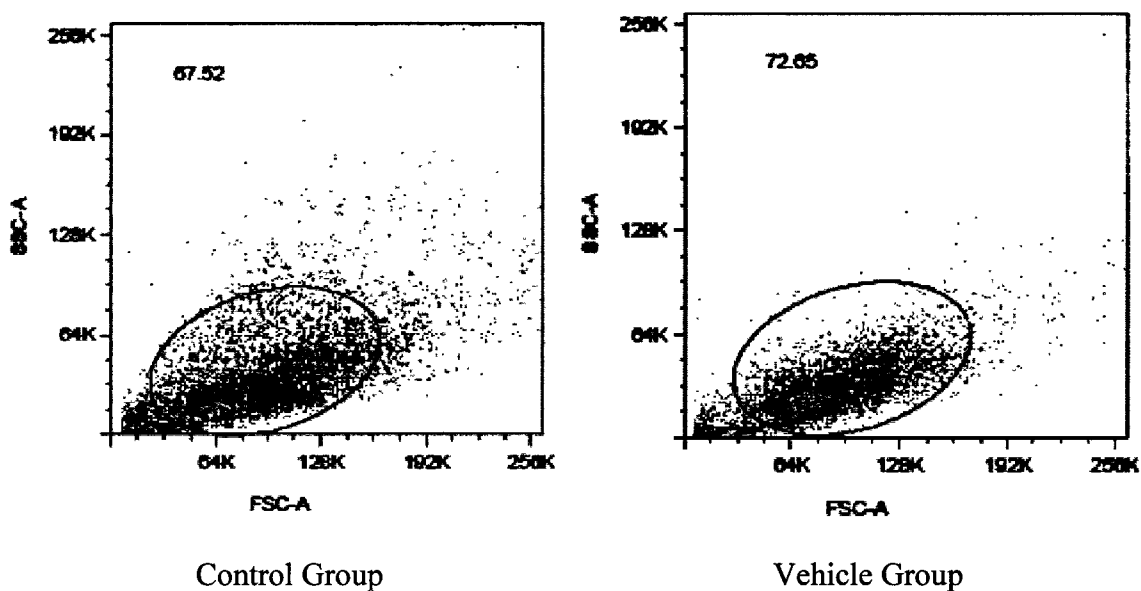
Figure 16. Histograms of 2% acetonitrile treated HCAEC.
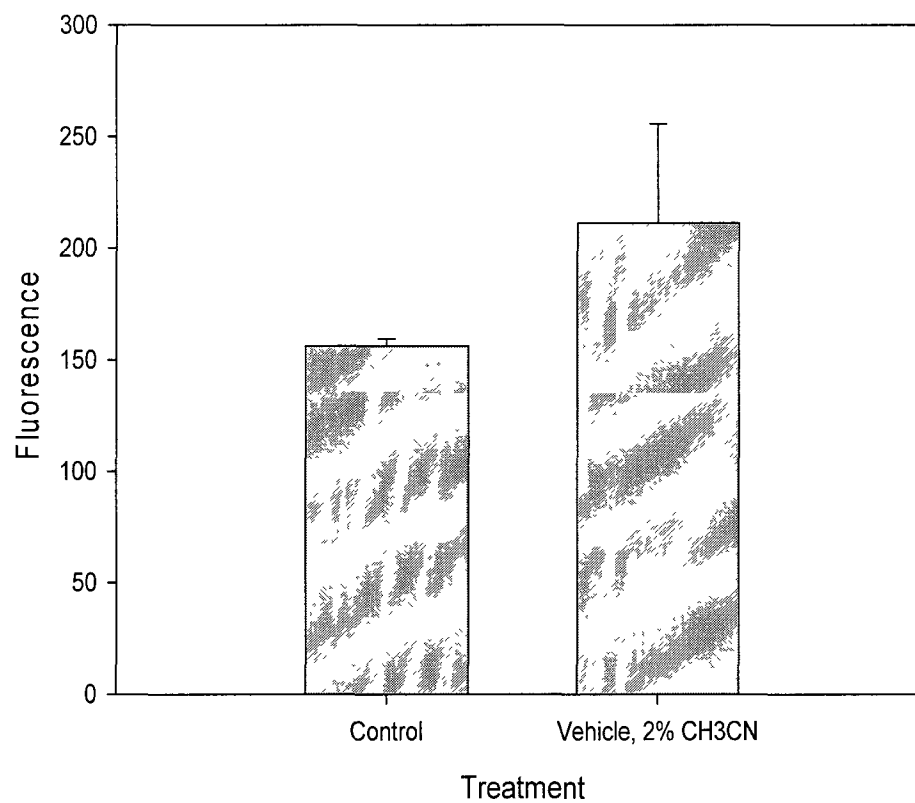
Figure 17. Vehicle effects on ROS generation. Cells treated with 2% acetonitrile for 0.5 hour as vehicle.
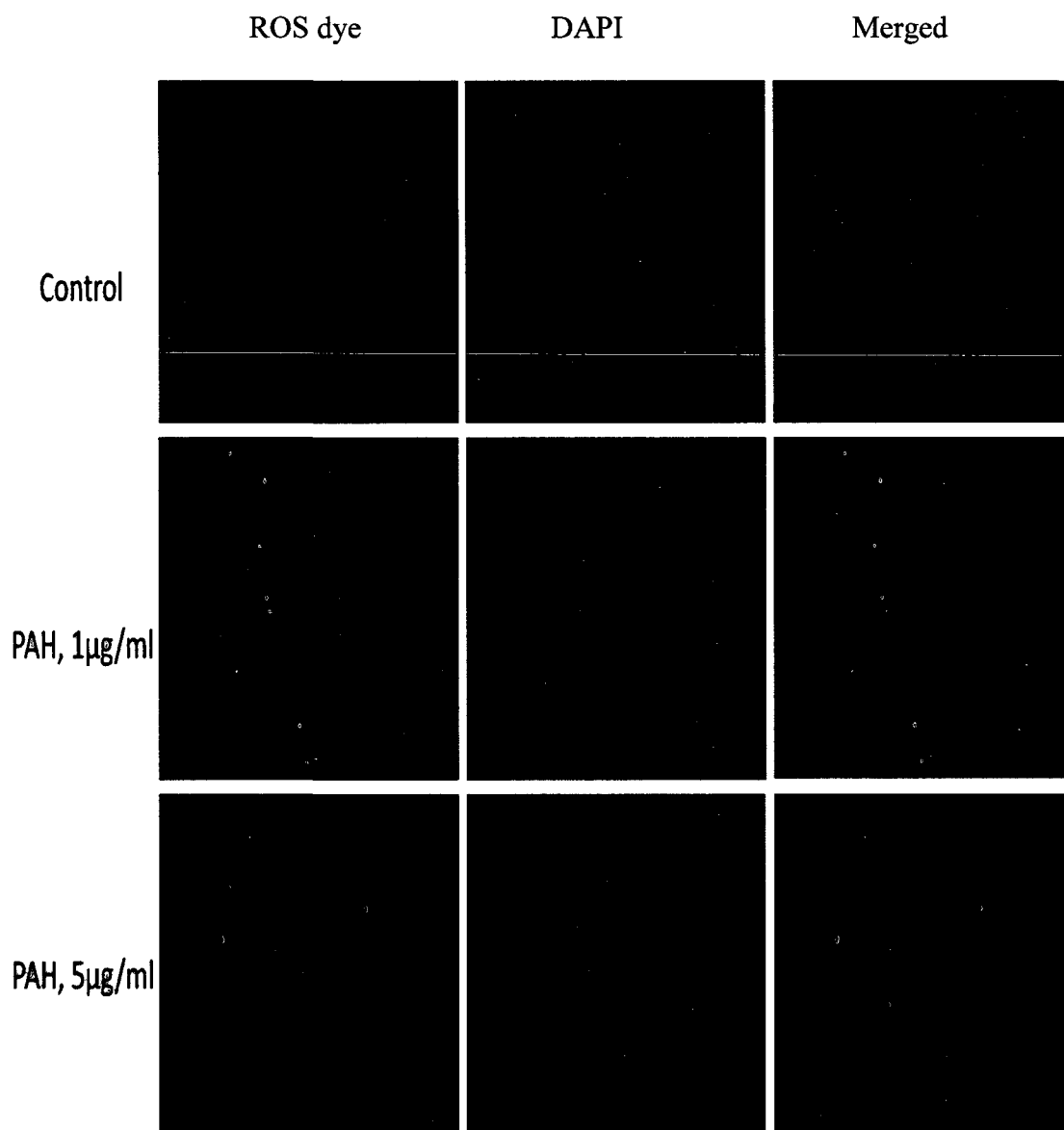
Figure 18. Fluorescent images of ROS after PAHs exposure. HCAEC were treated with 0 (control), 1 and 5 µg/ml PAHs for 0.5 hour. The cells were stained with carboxy-H_2DFFDA, then mounted with DAPI (blue: nucleus), cover slipped and viewed by a Nikon Eclipse 80 i microscope and cells were captured with a Cool SNAP EZ camera. (100x)

Figures 20 and 21 showed fluorescence generated in PAHs treated cells. A

representative overlapped results of PAHs treated cells showed that the fluorescence of

total cells shifted to the left (Figure 19). This indicates that the fluorescence reading

increased after PAHs exposure as compare with the control. Also, all of the HCAEC

exposed to 1, 5, and 12 µg/ml PAHs induced significant increases in ROS in HCAEC as

compared to the control (p values all < 0.05). The ROS level in the 1 µg/ml treated group

was more than three times higher than the control. 5 and 12 µg/ml PAHs exposure

induced 468% and 548% increases in ROS concentrations, respectively, as compared to

the control. Therefore, a dose-dependent pattern was observed.
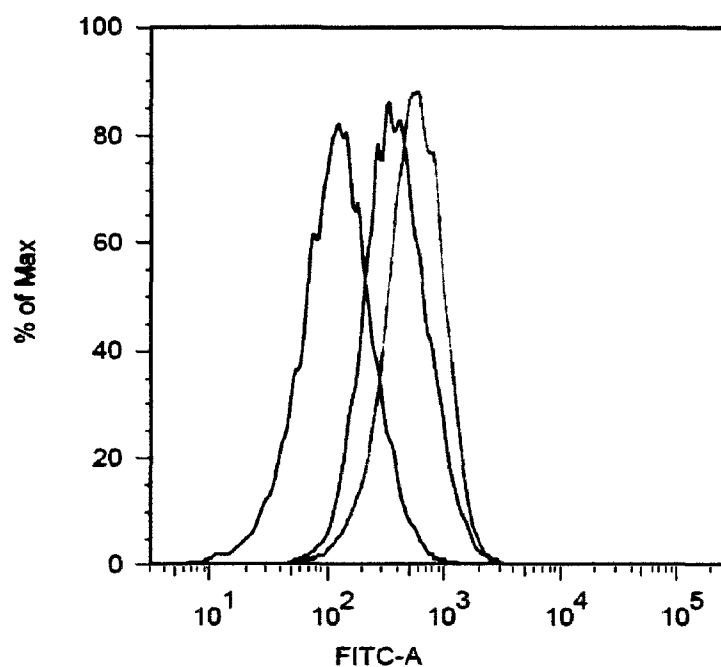
Figure 19. Oxidative effects of PAHs treatments. Gray, green and red lines represent cells treated with 0 (control), 1 and 5 µg/ml of PAHs, respectively. Data are the mean ± SEM of three independent experiments. * Indicates $p < 0.05$ in comparison with the control group.
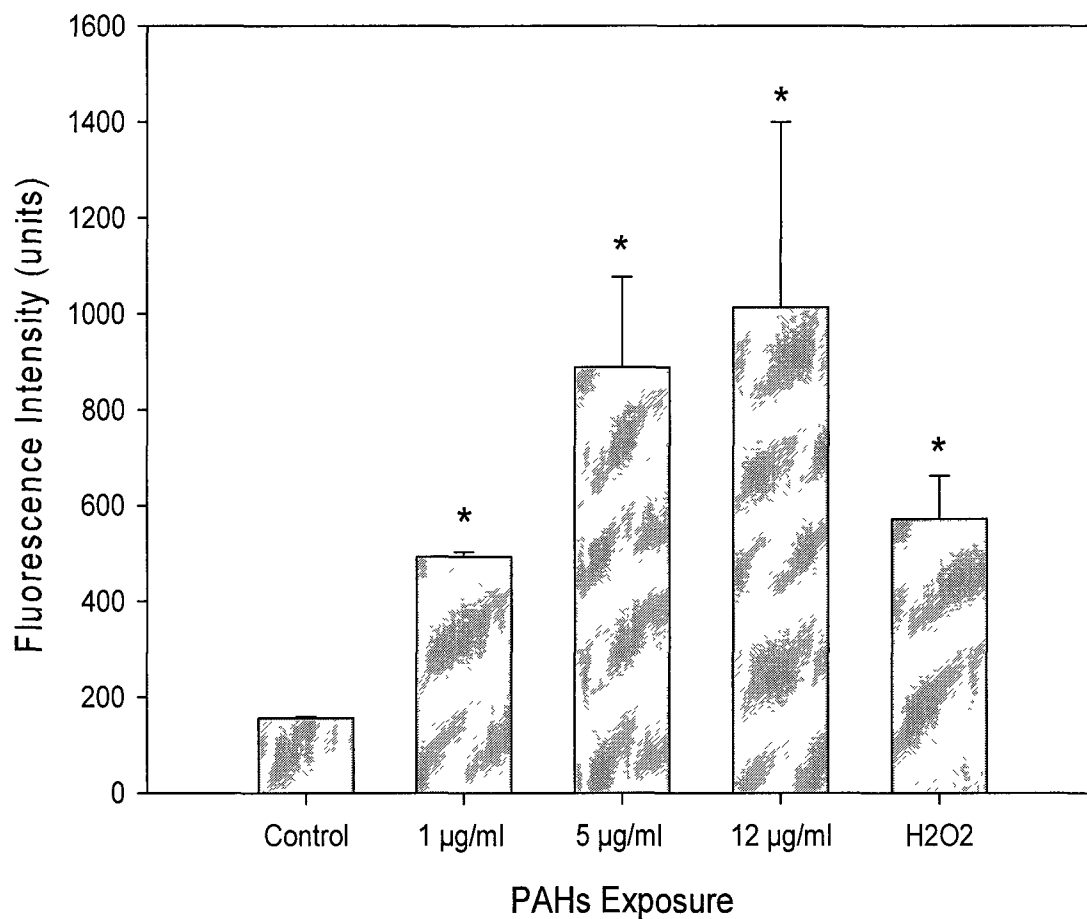
Figure 20. Concentration effects of PAHs on ROS production. HCAEC were treated with 0 (control), 1, 5 and 12 μg/ml PAHs for 0.5 hour. 100 μM/ml H_2O_2 were introduced to cells as positive control. Data are the mean ± SEM of three independent experiments. * Indicates $p < 0.05$ in comparison with the control group.

Figure 21 shows the effect of exposure duration on ROS generation. No significant differences were observed between 0.5 and 1 hour exposure at 5 µg/ml and 12 µg/ml PAHs. The results suggested that 0.5 hour PAH exposure could maximize the ROS generation in the endothelial cells.
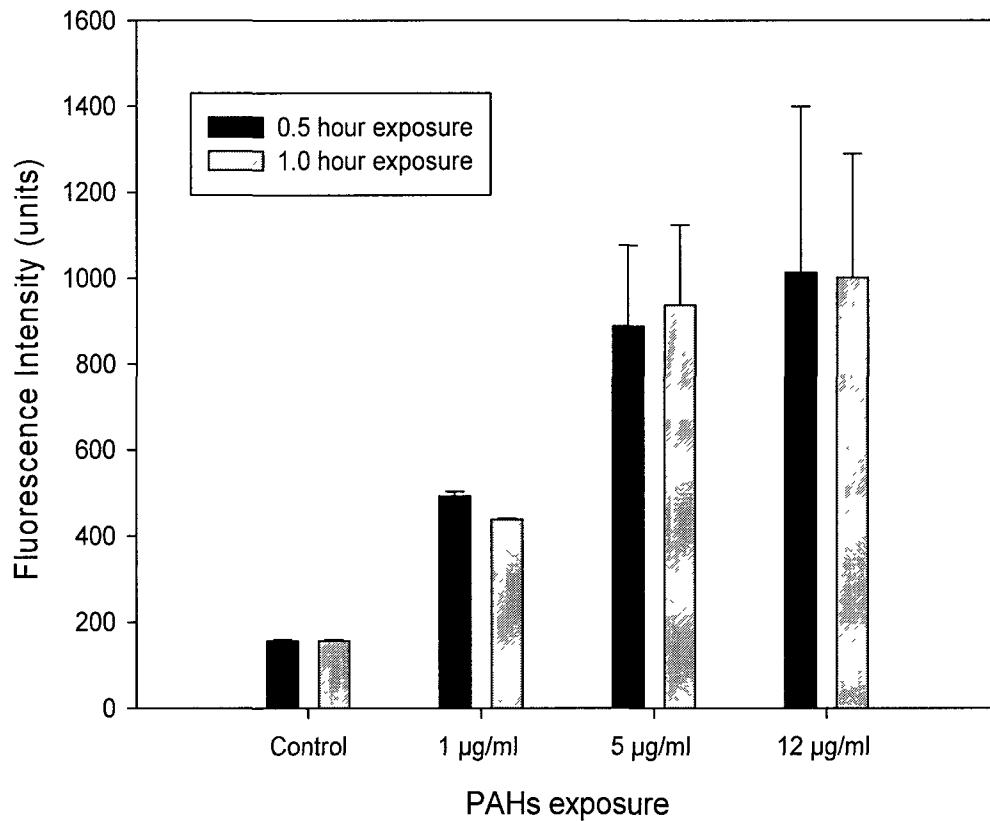
Figure 21. Time effects of PAHs on ROS production. Cells treated with 1, 5 and 12 µg/ml of PAHs for 0.5 and 1 hour, respectively. Data are the mean ± SEM of three independent experiments. * Indicates $p < 0.05$ in comparison with the control group.

DISCUSSION

Previous research had shown that PM extracts caused damage to vascular endothelial cells *in vivo* (Ichinose et al. 1995). Researchers also have found different results of the association between PM sizes and cytotoxicity (Churg and Brauer 1997). However, whether PM or PAHs causes direct cell damage in HACEC has not been clearly described. The study showed that PM induced acute cytotoxicity to endothelial cells. The findings were similar with other studies. The activation of human umbilical vein endothelial cells induced by $PM_{2.5}$ and PM_{10} has been reported to associate with an oxidative stress (Montiel-Davalos et al. 2010). Van Eeden reported that endothelial activation by PM may be due to pro-inflammatory factors released in the lung or to a direct contact of PM with the endothelium (van Eeden et al. 2005).

Fine particles with the size less that 3 μm compromised and damaged the cell membrane integrity to the degree that alters cellular morphology. Also, cell permeability was altered since cytosol was leaked out from HCACE. The cell injury could be associated with a decrease in the content of phospholipids (Prasad 1991). Particles were found to either bind outside cell membrane or enter into the cells. Subsequently, HCAEC viability was decreased after PM exposure. Although the mechanism of cell death was not investigated in this study, it is usually undergoing either apoptosis or necrosis. PM were proved to induce cell apoptosis in RAW 264.7 and J774 cells and human alveolar macrophages by activating the TNF-α-induced pathway (Huang et al. 2004; Alfaro-Moreno et al. 2002). Similar with PM, PAHs were observed to induce acute cytotoxicity, including the damage to the cell membrane integrity and decreased viability. PAHs were

likely the major component that contributes to acute cyotoxicity to endothelial cells induced by PM.

The ROS level is an important characteristic in the cellular responses to external stress. Moreover, increase in ROS level initiates various responses within the cell, including damage to proteins, DNA and lipid (Halliwell 2001). In order to measure the ROS level in HCAEC, two fluorescent probes were used in this study. Fluorescent dye, carboxy-H$_2$DCFDA, can be taken up by live cells and are able to emit fluorescence upon oxidation which can then be monitored using digital microscopy. After 12 hours of PM exposure, cell viability decreased, correlating with the increasing of ROS levels. ROS detection with a fluorescent microscopy after 24 hours of PM has no significant difference with the ones after 12 hours incubation. Possible reasons could be that the fine particles likely aggregate during the exposure or the fluorescence leaked out from the cells. The effects of PAHs with 1 and 5 µg/ml induced the increase of ROS were obviously noticed in HCAEC.

In order to quantify the level of ROS, the flow cytometry method was used with the fluorinated derivative, H$_2$DFFDA, which exhibits improved photostability compared to chlorinated fluorescein derivatives. This dye also shows exceptional retention in live cells due to the reaction of thiols with the fluoromethyl group which "traps" the difluorodihydrofluorescein in the cell. Oxidation by ROS yields a fluorescent difluorodihydrofluorescein which is detectible. After the cells treated with PAHs with the concentrations from 1, 5 and 12 µg/ml for different time periods, ROS intensity were significantly increased as compared to the control. The study clearly showed that PAHs induced the generation of ROS in the endothelial cell. PAHs on PM could be undergone

bio-transformation via cytochrome P450 to yield reactive electrophiles and superoxide hydroxyl radicals and continue the pathway involved with redox cycling to generates excessive concentrations of ROSs, such as H_2O_2, superoxide and hydroxyl radical (Shimizu et al. 2003).

The results demonstrated an imbalance of the production and the manifestation of ROSs, which can lead to oxidative stress to the cells. Excessive of the ROS production can disturb the redox status that lead to toxic effects to cells including alteration of cell morphology and the decrease in cellular viability.

In conclusion, PAHs induced acute cytotoxicity to endothelial cells via oxidative stress. PAHs on PM could increase the risk of the damage to endothelial cells in relation to cardiovascular disease. Thus, the control of emissions and compositions of PM is the important to the protection of public health..

CHAPTER III

POLYCYCLIC AROMATIC HYDROCARBONS CHANGE LIPID PROFILE AND NITRI OXIDE BIOAVAILABILITY TO ENDOTHELIAL CELLS *IN VITRO*

INTRODUCTION

Enhanced production or attenuated degradation of ROS leads to oxidative stress that affects endothelial and vascular function, which in turn contributes to vascular disease. Several pathological conditions increase the production of ROS in the vascular wall, such as diabetes and hypertension. These conditions are associated with endothelial dysfunction and cardiovascular disease. Among the arterial vascular tree, endothelium is the key member. Nitric oxide, a product of the normal endothelium, principally determined normal endothelial and vascular function (Montiel-Davalos et al. 2010), and increased in states of inflammation and contributed to oxidative stress in conjunction with other ROS (Lubos et al. 2008). Oxidative stress is proved to associate with lipid peroxidation as well. Lipid peroxidation is a major contributor to the related loss of membrane integrity, and with respect to pore formation and accumulation of unspecific lipid-protein adducts from aldehydic end products, such as malondialdehyde (Gujral et al. 2004). Therefore, the biological importance of lipids has drawn extensive attention to the analysis of lipid diversified molecular species. Latest characterizations by soft ionization Fourier transform ion cyclotron resonance mass spectrometry (FT-ICR-MS) have been increasingly utilized to profile global lipid distribution (Ivanova et al. 2001; Jones et al. 2005; Saghatelian et al. 2004; Yu 2006). For example, electrospray ionization FT-ICR-MS of total lipid extracts has been reported to be useful in detecting differences between

the distributions of highly heterogeneous mixtures of lipids found in eukaryotic cells (Ivanova et al. 2001). Thus, 12T FT-ICR-MS was performed in this study to access the lipid profiling on HCAEC.

Previous research showed that the bioactive lipids, especially oxidized phospholipids, can initiate and modulate many cellular events that attribute to atherosclerosis, suggesting that oxidized phospholipids would serve a biomarker for cardiovascular disease (Ashraf et al. 2009). Thus, this work aimed to evaluate 1) whether lipid peroxidation is linked to endothelial dysfunction in the HCAEC exposed to PAHs, and 2) whether the treatment of human endothelial cells with PAHs can alter the lipid profile and NO generation due to a disruption in redox balance.

EXPERIMENTAL PROCEDURES

Materials

A23187 calcium ionophore was obtained from Sigma-Aldrich (St.Louis, MO). Albumin

standard was obtained from Pierce (Rockland, IL). Apocynin was obtained from Fisher

Scientific (Pittsburgh, PA). β-Nicotinamide adenine dinucleotide phosphate, reduced tetra

(cyclohexylammonium) salt was obtained from Sigma-Aldrich (St.Louis, MO). 99.8%

chloroform was obtained from Acros (Thermo). Cell culture flasks and dishes were

obtained from Corning (Corning, NY). Cell lysis buffer was obtained from New England

Biolabs (Beverly, MA) and supplied as 10X cell lysis buffer. 8 chamber tissue culture

treated glass slide was obtained from BD Falcon (Bedford, MA). Comassie protein assay

kit was obtained from Pierce (Thermo, Rockford, IL). Disel particulate matter was

obtained from National Institute of Standards and Technology (NIST, Geithersburg, MD).

Dimethyl sulfoxide (DMSO) was obtained from Sigma. Ethylenediaminetetraacetic acid

(EDTA) was obtained from Sigma. Ethylene glycol-bis(2-aminoethylether)-N,N,N',N'-

tetraacetic acid (EGTA) was obtained from Sigma. Glass tubes, borosilicate (16x100mm),

were obtained from Fisher. Human coronary artery endothelial cells (HCAEC) were

purchased from Cell Applications, Inc. (San Diego, CA) and grown in culture at 37°C

and 5% CO2 cells were grown in Medoendo Eell Growth Media. Hank's balanced salt

solution, calcium- and magnesium-free (HBSS) was obtained from Mediatech Cellgro

(VA).30% H_2O_2 was obtained from Fisher Scientific. Homogenizer was obtained from

Fisher Scientific. H_2DFFDA was obtained from Invitrogen. Isopore membrane filters,

3.0μm TSTP and 1.2 μm RTTP, were obtained from Millipore (Billerica, MA). 8-

Isoprostane Express EIA Kit (Catalog #516360) was obtained from Cayman Chemical

(Ann Arbor, MI). Lactate dehydrogenase (LDH) Kit (Cat # 04744926001) was obtained

from Roche. β-Nicotinamide adenine dinucleotide phosphate, reduced

tetra(cyclohexylammonium) salt (NADPH) was obtained from Sigma. 99% methyl

alcohol was obtained from Acros (Thermo). Mounting medium for fluorescence with

DAPI was obtained from Vector (Burlingame, CA). Nω-Nitro-L-arginine methyl ester

hydrochloride (L-NAME) was obtained from Sigma-Aldrich (St.Louis, MO).

Polypropylene centrifuge tubes (15ml) were obtained from Corning Inc. (Corning, NY).

Polycyclic aromatic hydrocarbons were obtained from Restek (Bellefonte, PA). Sodium

dodecylsulfate (SDS) was obtained from American Bioanalytical. Sodium hydroxide

(NaOH), 10N solution, 30% w/w, was obtained by Fisher Scientific. Thiobarbituric Acid

Reactive Substances (TBARS) Assay Kit (Cat.# 0801192) was obtained from

ZeptoMetrix Corporation (Buffalo, NY). Total Nitric Oxide Assay Kit (Lot # KG134678)

was obtained from Thermo Scientific (Rockford, IL). Triton-X100 was obtained from

Fisher Scientific. Trypan blue solution (0.4%) was obtained from Sigma-Aldrich

(St.Louis, MO). Phosphate buffered saline 10X was obtained from Fisher Scientific.

PTFE cap and target vials were obtained from Fisher scientific. All aqueous solutions

and reagents were prepared in deionized distilled water using ELGA Purelab system from

SIEMIENS.

Cell Culture and Preparation

Endothelial cells are economical alternative, suitable for studies of endothelial

functional and endothelial metabolism. Changes in structure and function of these cells

have been linked to vascular diseases such as atherosclerosis, and hypertension. Human

coronary artery endothelial cells (HCAEC) used in this study was isolated from normal human coronary arteries from Cell Application (San Diego, CA). HCAEC were grown in Mesoendo Cell Growth Medium that is fully supplemented with fetal bovine serum, growth factors, trace elements and antibiotics. The cells in culture flasks were placed in an incubator at 37 °C with a humidified atmosphere of 5 % CO_2. Cells were preserved and stored with liquid nitrogen in a cryosystem (Cryogenic locator, Thermo).

HCAEC was cultured for treatment when cells are about 80-90% confluent. Cells were used for all experiments on the passages 5 to 15. Active proliferation cells were exposed to fine particle or PAHs solutions prepared as described below. After exposure, cells were harvested from cultured flask. This involves removal of media from flask, a rinse with Hank's Balanced Salt Solution 1X, trysin EDTA 1X 0.25 % trypsin/2.21 mM EDTA in HBSS addition and Mesoendo Cell Growth Medium addition. HCAEC preparation prior to bioassays involves centrifugation at 1092 rpm (200g), removal supernatant, followed by HBSS wash twice. Cell count was performed using a hemacytometer.

Polycyclic Aromatic Hydrocarbons Preparation

EPA method 8310 PAH Mixture was obtained from Restek Corporation. Acetonitrile with composition of 99.1 % was used as solvent. Certificate of analysis provided PAH compound and concentration (Appendix D). Ultrasonication was used to remove air bubbles or to breakup agglomerates before loading 1 ml of the sample into disposable polystyrene cuvettes. The PAH solution was prepared and diluted immediately before cell exposure, and diluted as required. Cells were exposed to PAH

with variable factors of exposure, including the concentration and the duration time of exposure.

Measurement of Thiobarbituric Acid Reactive Substances

Thiobarbituric acid reactive substances (TBARS) were used as a colorimetric method to detect malondialdehyde (MDA), an index of lipid peroxidation.

The measured MDA concentration was followed by comparison to linear regression analysis, and was expressed as MDA equivalents and normalized to total protein in each sample. In brief, cell homogenization was mixed with the commercially kit, including butylated hydroxytoluene, thiobarbituric acid and trichloroacetic acid. The mixture was boiled for 1 hour at 95 °C, followed by centrifugation after cool down. The supernatant was measured by a spectrophotometer at the 535 nm. A standard curve was made based on a series of known MDA concentrations. MDA level was expressed in nmol/ml/mg after the adjustment of protein concentration.

Protein Measurement

The protein level was estimated by Bradford method using bovine serum albumin (BSA) as a standard. Dilute the 2 mg/ml BSA standard to make a standard curve from 2.5-2000 μg/ml in 0.05 N NaOH. Add 5 μL of standard, resuspended protein pellet to each well of a micro plate in duplicate. Add 250 μL of 1X coomassie protein assay reagent to each well of the plate. Incubate at room temperature for at least 5 min. Read on a micro plate at 600 nm.

Lipid Extraction

The entire cellular lipids were extracted based on the process that the volumes of chloroform, methanol and water, before and after dilution, were kept in the proportions of 1:2:0.8 and 2:2:0.8, respectively. The lower chloroform layer containing lipids were aliquotted as 10% of total sample into glass vials. The vial was placed under a stream of nitrogen for evaporation and dryness. Briefly, HCAEC were harvested from the flasks with scraper, and then were transferred and centrifuged for 10 minutes at 1500 rpm. The supernatant was discarded and the pellet was resuspended in 0.8ml H_2O. Spin gently to mix the cell pellet and transfer the mixture to a homogenizer. Cell lipids were homogenized for a few minutes with 2ml methanol and 1ml chloroform. Then additional 1ml chloroform was added and was homogenized for 30s following spinning at a high speed. After allowing a few minutes for separation and clarification, the alcoholic layer on the top was removed with long glass pipettes. Remaining chloroform layer containing the purified lipid were collected and evaporated to dryness under a stream of nitrogen at room temperature. Lipids were stored at -80 °C if not used immediately.

Lipid Profiling Assessment

A Bruker 12 Tesla Apex Qe Fourier Transform Ion Cyclotron Resonance Mass Spectrometer (12T FT-ICR-MS) at ODU's COSMIC LAB was applied to obtain exact chemical formulae for organic compounds under 2000Da and to profile lipid distribution. The high-resolution capability of this instrument offers detection of ions in a wide m/z range. The ion funnel with the electrospray and nanospray provided both positive and negative ion runs for identification of polar compounds.

In this study, the 12 T FT-ICR-MS was performed on the lipid extracts of HCAEC to demonstrate its lipid profiling capability. The dry lipid sample was prepared by chloroform and methanol with the extraction method described as above, and then it was resuspended in running solvent before injecting in the FT-ICR-MS. The solvent of methanol with 0.1% (v/v) formic acid was used for the positive ion runs, and that of methanol with 0.1% (v/v) ammonium hydroxide was for the negative ion runs.

After screening the raw data, spectrum was calibrated and the peaks were separated to determine molecular mass while molecular formulas were assigned. The molecular formulas were used to generate the van Krevelen diagram, a two-dimensional plot, to clarify where the lipids classes were located and to recognize oxidation/reduction pathways. And then the Matlab program was used to analyze the atoms (C, H, N, O, S, and P) in negative ion mode and to compare them among treatment groups. Manipulations were done after importing data into Excel to find out the oxidative effects of PAH on lipids in endothelial cells.

Measurement of Total Nitric Oxide

Total nitric oxide in the endothelial cells following PAHs exposure was assed quantitatively using Griess reagent kit (Thermo, KG 134678) (Ghosh et al. 2009). NO concentration was determined by measuring the content of NO_2^- in cell culture supernatants, Griess reagents was used for spectrophotometric determination of NO_2^-. Because of the instability of NO in physiological solution, NO oxidizes rapidly to the mixture of NO_2^- and NO_3^- in the presence of oxygen. To avoid underestimating NO, NO_3^- was converted to NO_2^- by nitrate reductase, thereby yielding measurement of total

NO. The colorimetric assay of nitrite (NO_2^-)/ nitrate (NO_3^-) provided high sensitivity at lower Arginine concentrations.

HCAEC were cultured in a 96-well culture plate at a density of 2×10^4 cells/ml, and were treated with 1 µg/ml, and 5 µg/ml PAHs for 0.5 hour incubation. Cell culture supernatants were collected and loaded in a polystyrene black clear bottom 96- well plate with 100µl/well, followed by 25 µl of diluted NADH and 25 µl of nitrate reductase enzyme dilution added into each well. The plate was shaking gently to mix well and was incubated for 0.5 hour at 37 °C with a plate sealer. Then the plate was incubated at room temperature for 10 minutes after adding 100 µl of Griess reagent into each well. The reaction produced a chromophore that was measured at 540 nm. The amount of nitrite accumulated was calculated (in µM) by comparison with standard curve constructed with known concentrations of sodium nitrite prepared in the cultured medium.

Detection of Endothelial Nitric Oxide Synthase Activity

A fluorimetric cell-associated nitric oxide synthase system was used to detect NOS activity (Sigma, FCANOS1). The method is based on the principle that a detectable fluorescent DAF-2T is converted from the non-fluorescence DAF-2DA at the presence of NOS derived NO. A plate reader at the excitation wavelength of 450-495 nm and an emission wavelength of 505-550 nm measured the fluorescent product. Relative units was reported to reflect NOS activity, because most fluoresce is affected by numerous factors that vary from the environmental conditions of experiments, including excitation light quality and quantity, instrument geometry and detector characteristics. The NOS activity was adjusted to the total protein. The protein level and activity of NOS was

studied simultaneously. A23187, also known as calcium ionophore was used as NOS

stimulator to increase NO production. Diphenyleneiodonium chloride (DPI) was used as

an NOS inhibitor in the positive group to reduce NO generation.

Statistical Analysis

Statistical analysis was performed using Sigma-Plot software. All experiments

were carried out in triplicate, and results were expressed as means ± standard error of the

mean (SEM). Comparisons involving three or more groups were evaluated using one-

way ANOVA and an appropriate *post hoc* comparison. Instances involving only two

comparisons were evaluated with a Student's *t*-test. Differences among means were

considered statistically significant by the criterion of probability P value ≤ 0.05.

RESULTS

Lipid peroxidation measurements in HCAEC

Base on the standard curve of MDA, excellent quality control (R^2= 0.99) was generated for the following analysis.

After exposure, MDA was significantly increased in the 1 μg/ml PAHs treated groups (69.9%, p value = 0.001) after 0.5 hour of treatment as compared to the control (Figure 22). Moreover, the increase of MDA released from 5 μg/ml PAHs treated HCAEC was significantly higher than the control (161.5%, $p < 0.001$). However, no significant difference was observed between 1 and 5 μg/ml PAHs treated groups. From the results, PAHs induced MDA production in endothelial cells followed a concentration-dependent manner. In addition, increased MDA production in HCAEC had the same trend with the increase in ROS generation (Figure 23).

Effects of PAHs on NO level

The present study measured the total nitrite as the indicator to estimate the NO level in HCAEC. Base on the standard curve of nitrite, excellent quality control (R^2= 1) was generated for the following analysis.

After exposure, there was an increase in nitrite concentration in the 1 μg/ml PAHs treated groups (52.7%) after 0.5 hour of treatment as compared to the control (Figure 24). Moreover, the increase of NO release from treated HCAEC treated by 5 μg/ml PAHs was significantly higher (74.2%) than the control (p value = 0.003). The increased total nitrite generation in HCAEC had the same trend with the increase in ROS generation (Figure 25).
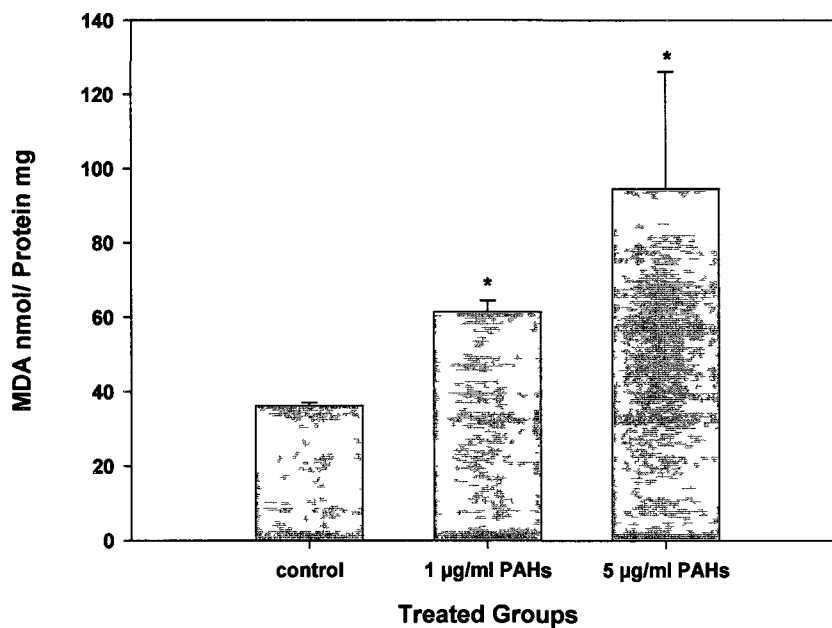
Figure 22. Lipid peroxidation measurement. HCAEC were exposed to 0 (control), 1 µg/ml and 5 µg/ml PAHs for 0.5 hour. After incubation, MDA released into the cell growth medium was determined. Data are the mean ± SEM of three independent experiments. * Indicates $p < 0.05$ in comparison with the control group
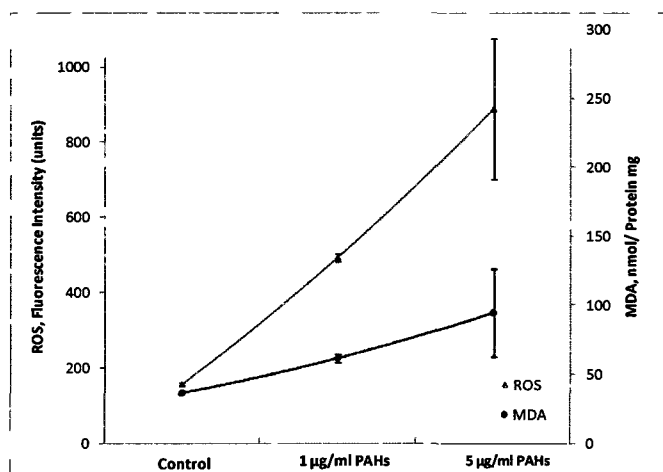
Figure 23. Effects of PAHs on MDA level and ROS.
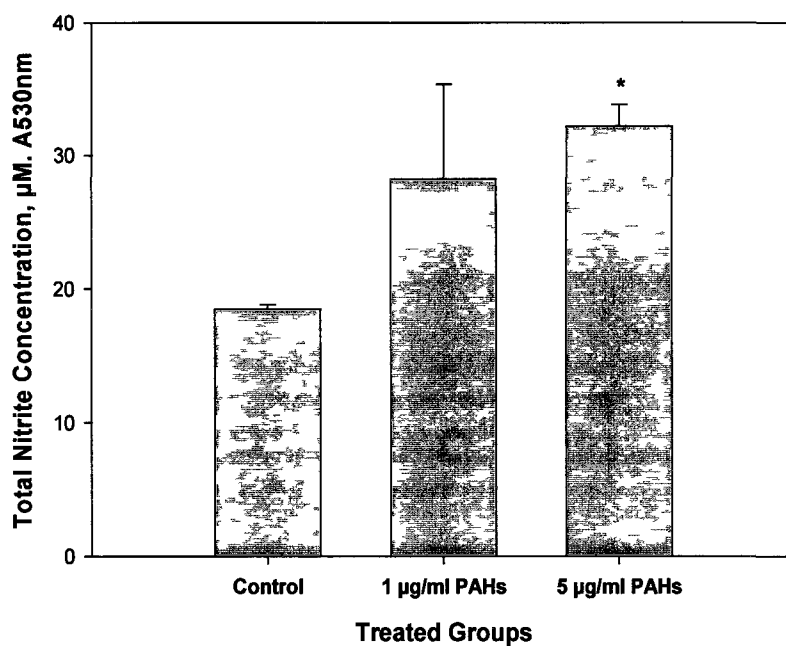
Figure 24. PAHs effects on NO level. HCAEC were exposed to HCAEC were exposed to 0 (control), 1 µg/ml and 5 µg/ml PAHs for 0.5 hour. After incubation, total nitrite released into the media was determined. Data are the mean ± SEM of three independent experiments. * Indicates $p < 0.05$ in comparison with the control group
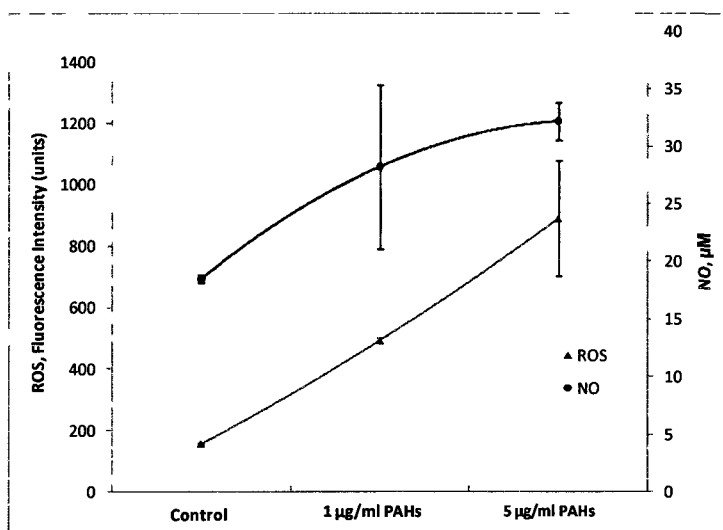
Figure 25. Effects of PAHs on NO level and ROS.

Effects of PAHs on eNOS activity

This study describes comparative in vitro studies of the kinetics patterns of

calcium ionophore (A23187)-stimulated NO release was associated with accelerated

decomposition of NO from the endothelial cells. After control cells incubated with

A23187, a rapid increase of fluorescence reading, 35.1% (p value = 0.01) was observed

in comparison with control group. This result confirmed the stimulating effects of

A23187 to eNOS.

1 μg/ml of PAHs induced an increase of 12.4% in eNOS activity in HCAEC,

compared to control, while the eNOS activity in 5 and 12 μg/ml of PAHs treated groups

were observed significantly increases with 13.8% and 31.2% (p values were 0.04 and

0.02, respectively). Percentages increase in eNOS activity induced by 5 and 12 μg/ml

PAHs were significantly higher than 1 μg/ml of PAHs treated group (p values were 0.02

and 0.004, respectively). The eNOS activity level observed after incubated with 12

μg/ml of PAHs was significantly higher than 5 μg/ml of PAHs (15.2%, p value was

0.007). Therefore, PAHs modulated eNOS activity in endothelial cells followed a

concentration-dependent manner.
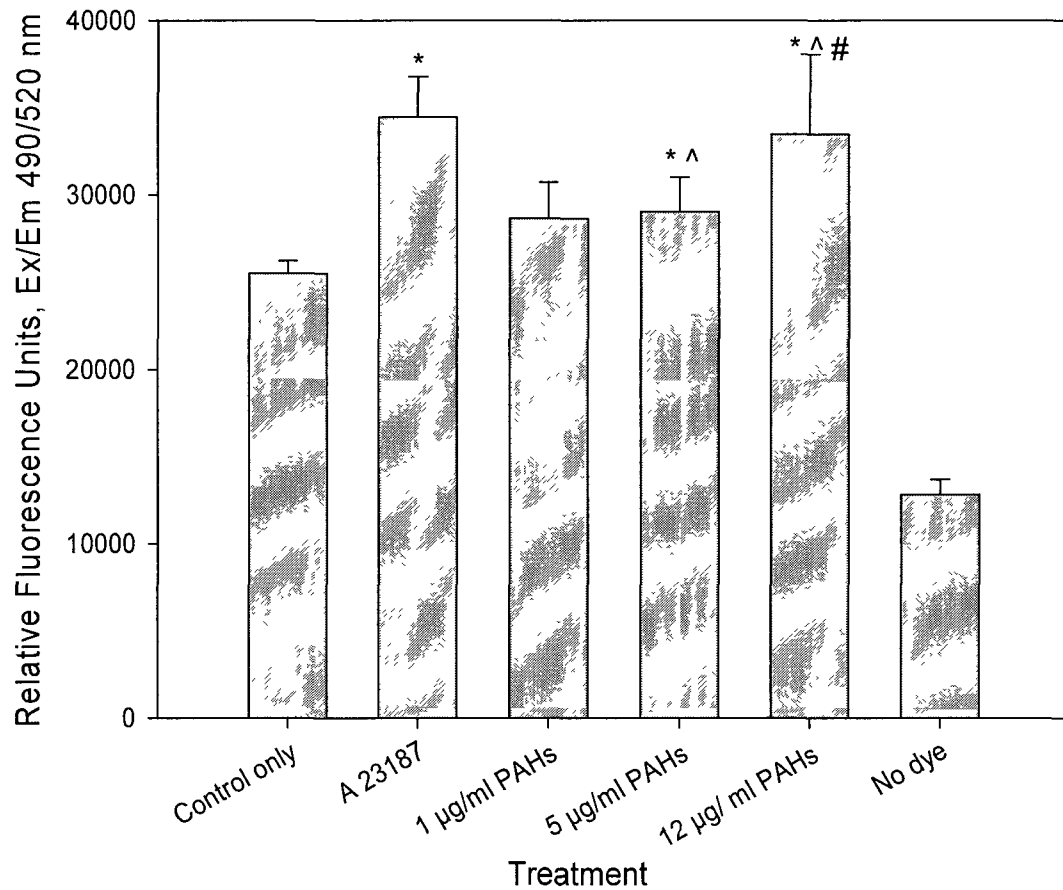
Figure 26. PAHs effects on eNOS activity. HCAEC were exposed to 0 (control), 1, 5 and 12 µg/ml PAHs for 0.5 hour. Cells incubated with 5 µM A23187 for 10 minutes as positive control. Cells treated without dye, DAF-2DA, were used as negative control. Data are the mean ± SEM of three independent experiments. * Indicates $p < 0.05$ in comparison with the control group. ^ Indicates $p < 0.05$ in comparison with the 1µg/ml PAHs treated group. # Indicates $p < 0.05$ in comparison with the 5 µg/ml PAHs treated group

Effects of PAHs on NO Levels in HCAEC

L-NAME was used as the inhibitor of eNOS. After PAHs exposure, the NO

levels increased in a concentration dependent manner, while the L-NAME decreased the

NO generation in HACEC treated with PAHs. In addition, a significant decrease of NO

was observed in the 5 μg/ml PAHs treated group, which indicating that the L-NAME

modulated eNOS played an important role in regulating the NO level in HCAEC. This

data supported the results generated from the last set of experiment that PAHs activate

eNOS activity in endothelial cells. The altering eNOS activity induced by PAHs is

involved with altering NO bioavailability.
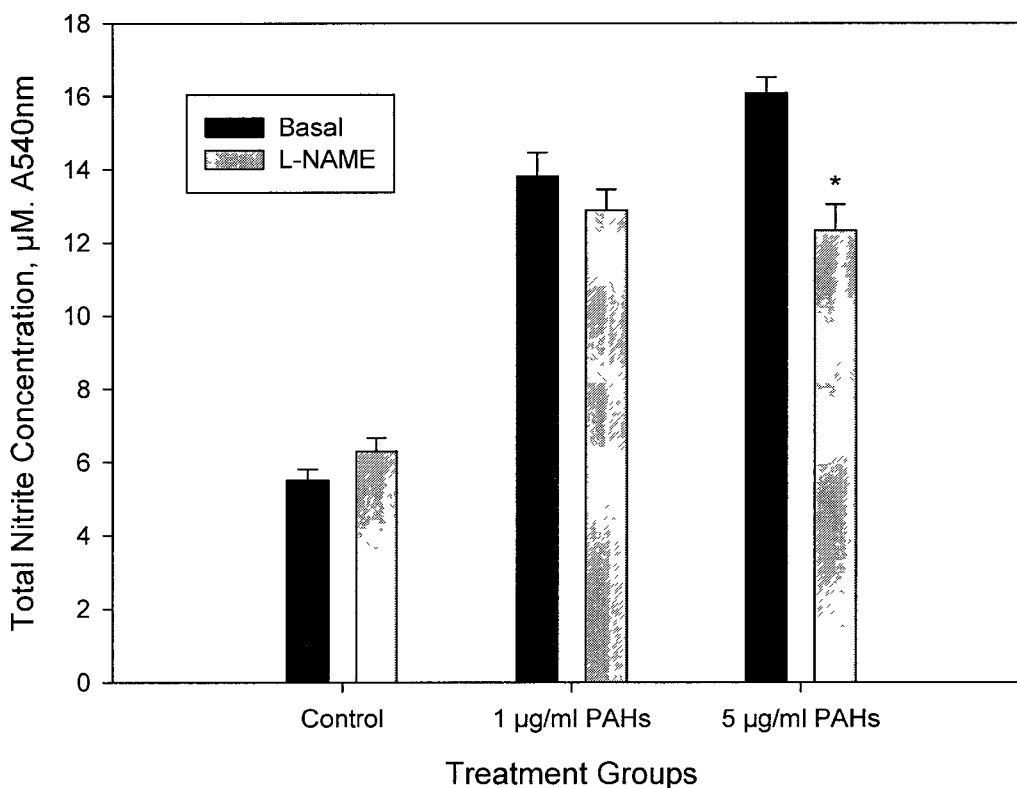
Figure 27. Effects of L-NAME to HCAEC

Effects of NADPH on NO Levels in HCAEC

NADPH was used to investigate whether superoxide induced by PAHs is

involved with NO bioavailability. After PAHs exposure, NO levels increased with a

concentration-dependent manner. However, with NADPH exposure, the cells exposed to

both 1 and 5 μg/ml PAHs had significantly lower the NO levels as compared to the

control. This result confirmed that superoxide can be generated by PAHs exposure and

directly oxidize NO. At the same time, other mechanisms existed and possibly up-

regulate eNOS that dominates biological reactions in the cells treated by PAHs. Thus, in

overall, NO levels were increased after PAH exposure.
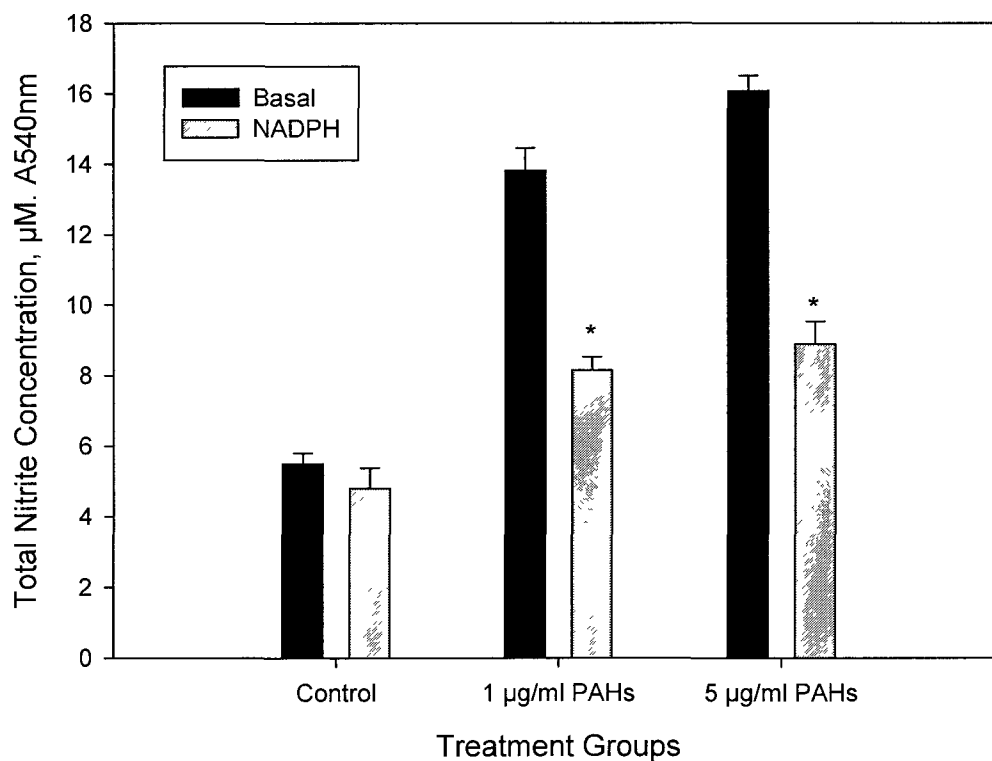
Figure 28. Effects of NADPH on HCAEC

Effects of PAHs to lipid profile in HCAEC

Van krevelen diagram was commonly used as an approach to visalized

complicated mass spectra in the ultrahigh-resolution ESI-MS analyses (Kim et al. 2003).

With this approach, complicated spectra can be plotted in a way that allows for possible

reaction pathways to be identified and qualitative analyses on major classes, such as

lipids. In the present study, van Krevelen diagrams revealed PAH-exposed groups had

cluster molecules, defined as lipids according to the compound classes.

Figure 29 displayed the calibrated mass spectrum of lipids in the control and 1

μg/ml PAHs treated group from negative iron run. Over 600 peaks are detected in the

mass range from 200 to 700 *m/z*. The lipid extracts may contains other biomaterials or

biodegraded residues, resulting in a multitude of peaks being observed at each nominal

mass (see table 3). The elemental compositions of peaks are calculated from the

corresponding exact mass numbers obtained from the calibrated spectrum, from which, C,

H, O, and N atoms are used to assign the most probable elemental formulas. The

compositions can be assigned with usually < 1 ppm error, and the numbers of atom used

to set during the calibrations are C: 4-65; H: 4-150; O: 0-20; N: 0-4; P: 0-4; S: 0-1. Some

peaks with higher molecular weight, such as over 400 *m/z*, may have more than one

possible elemental formula. In order to resolve this problem, Kendrick mass defect

analysis was used to determine the assigned elemental formula to make the compound

biological and chemical available, which was done previously (Stenson et al. 2003;

Hughey et al. 2001). To show the complexity of the spectrum, the region of 219-340 *m/z*

is selected and expanded (Figure 29). Representative peaks of lipids in 1 μg/ml PAHs

treated HCAEC are detected and assigned (Table 3). Therefore, examining individual

peaks in the entire mass range and extracting information, such as the distribution of the class of the compounds from the spectra, represents a tremendous time and effort involved.

Table 3. List of representative peaks indentified in the 1 µg/ml PAHs treated HCAEC

Observed mass, m/z	Proposed mol formula							Theoretical mass, m/z	Difference from thero value (ppm)
	C	H	H+1	N	O	S	P		
219.175402	15	23	24	0	1	0	0	219.175439	-0.2
221.154692	14	21	22	0	2	0	0	221.154703	-0.1
227.201675	14	27	28	0	2	0	0	227.201654	0.1
233.154725	15	21	22	0	2	0	0	233.154703	0.1
234.186182	15	24	25	1	1	0	0	234.186338	-0.7
235.170223	15	23	24	0	2	0	0	235.170354	-0.6
239.12872	13	19	20	0	4	0	0	239.128883	-0.7
239.165087	14	23	24	0	3	0	0	239.165268	-0.8
239.201475	15	27	28	0	2	0	0	239.201654	-0.7
241.144575	13	21	22	0	4	0	0	241.144533	0.2
241.180867	14	25	26	0	3	0	0	241.180918	-0.2
241.217275	15	29	30	0	2	0	0	241.217304	-0.1
242.176173	13	24	25	1	3	0	0	242.176167	0
247.170347	16	23	24	0	2	0	0	247.170354	0
249.149563	15	21	22	0	3	0	0	249.149618	-0.2
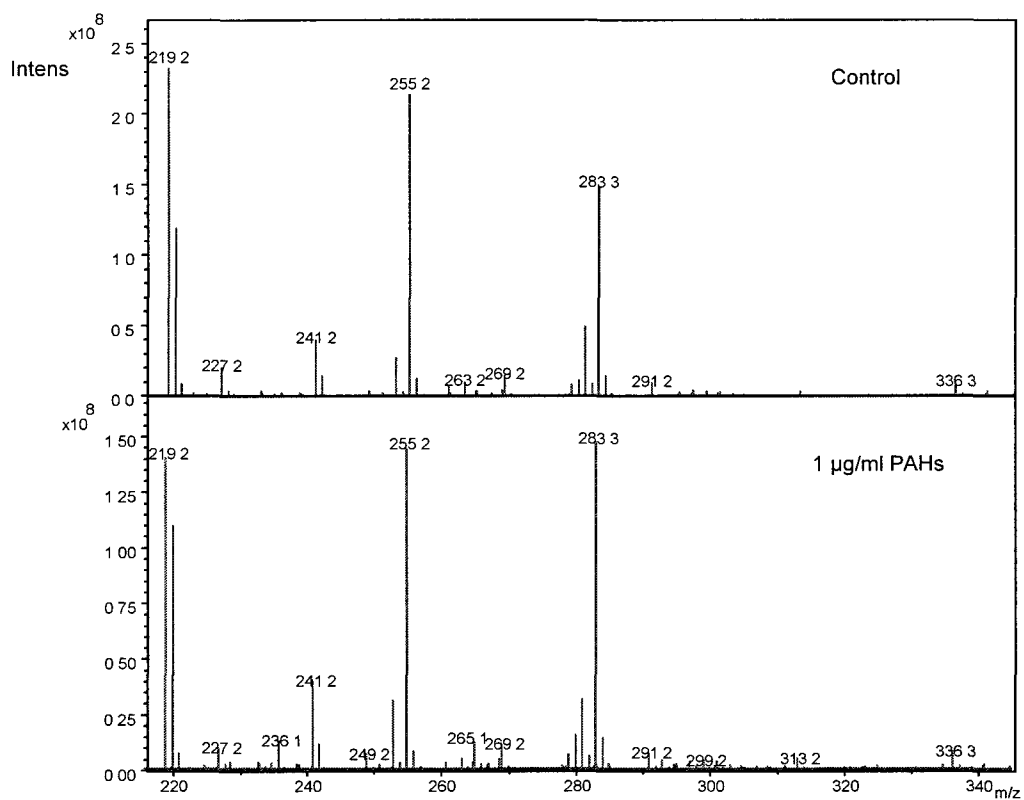
Figure 29. The expanded view of 219.0-340.0 *m/z* region of the ultrahigh-resolution mass spectrum of HCAEC lipids

The van Krevelen diagram of ultrahigh-resolution mass spectrometric data was plotted using the molar ratio of hydrogen to carbon (H/C) as the y-axis and the molar oxygen to carbon ratios (O/C) as the x-axis. In the van Krevelen diagram, major biomaterial classes of compounds locate in specific plot areas on the diagram since they have their own characteristic H/C and O/C ratios. The lipid data of HCAEC was displayed and circled in Figure 30. The outliers were possibly derived from noise spikes in the diagram, or some contamination compounds that remained after lipid extraction.

In the PAHs treated groups, the number of molecules clustered with the mole O/C and H/C rations between 0 and 0.4, and 1.5 and 2.2, are much higher than that in the control, indicating that PAHs increased the component numbers of lipids. In the van Krevelen plot, trend along the line can be used to indicate the structural relationships among families of compounds generated by reactions that involve loss or gain of elements in a specific molar ratio (Kim et al. 2003). The plot revealed that PAH exposure induced various chemical reactions in HCAE. For example, the pink line in Figure 31 showed the oxidation and/or reduction that occurred after PAH exposure. Also, the methylation and/or demethylation reaction took place marked as the blue line.
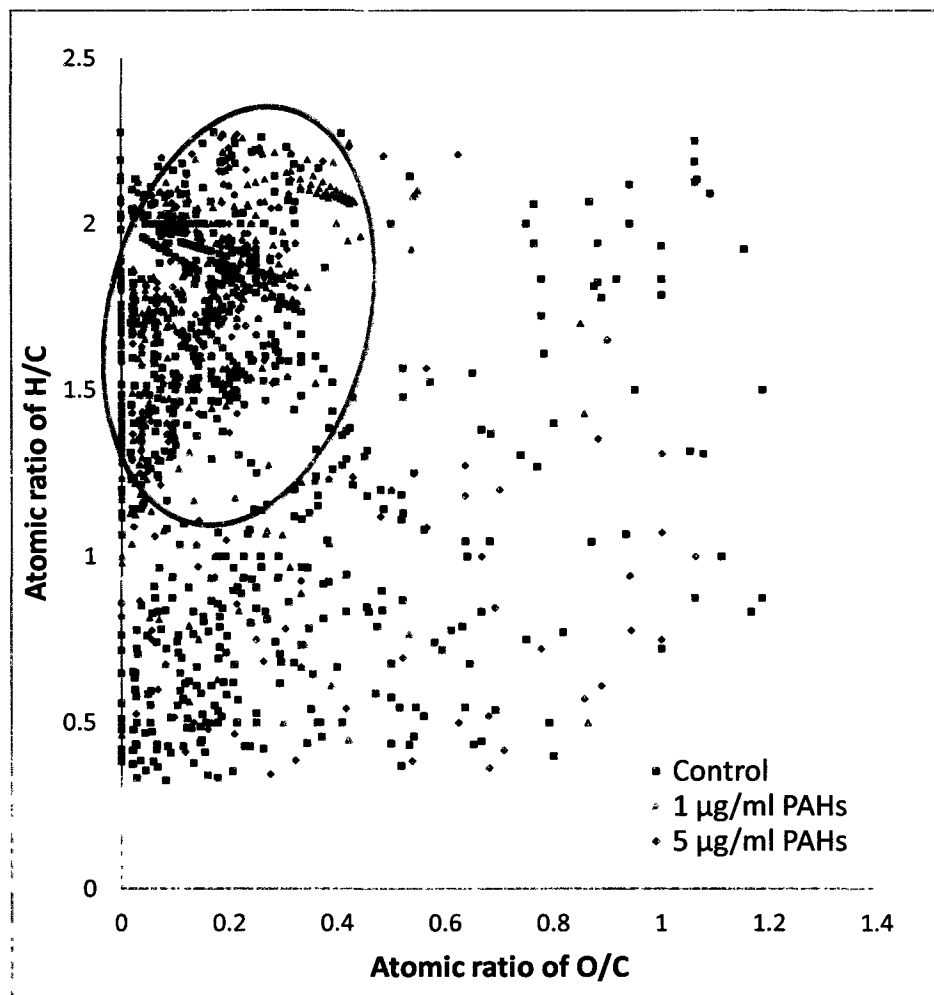
Figure 30. Lipid data plot in the van Krevelen diagram. Lipids of cell membrane were extracted by chloroform and methanol, and then analyzed using the FT-ICR-MS to separate peaks. The separate peaks were used to determine molecular mass while molecular formulas were assigned. After screening the row data, the Matlab program was used to analyze the atoms (C, H, N, O, S, and P) in negative ion mode and to compare them among treatment groups. Van Krevelen diagram were generaged based on O/C and H/C ratio. Lipid compound classes are represented by circles overlaid on the plot.
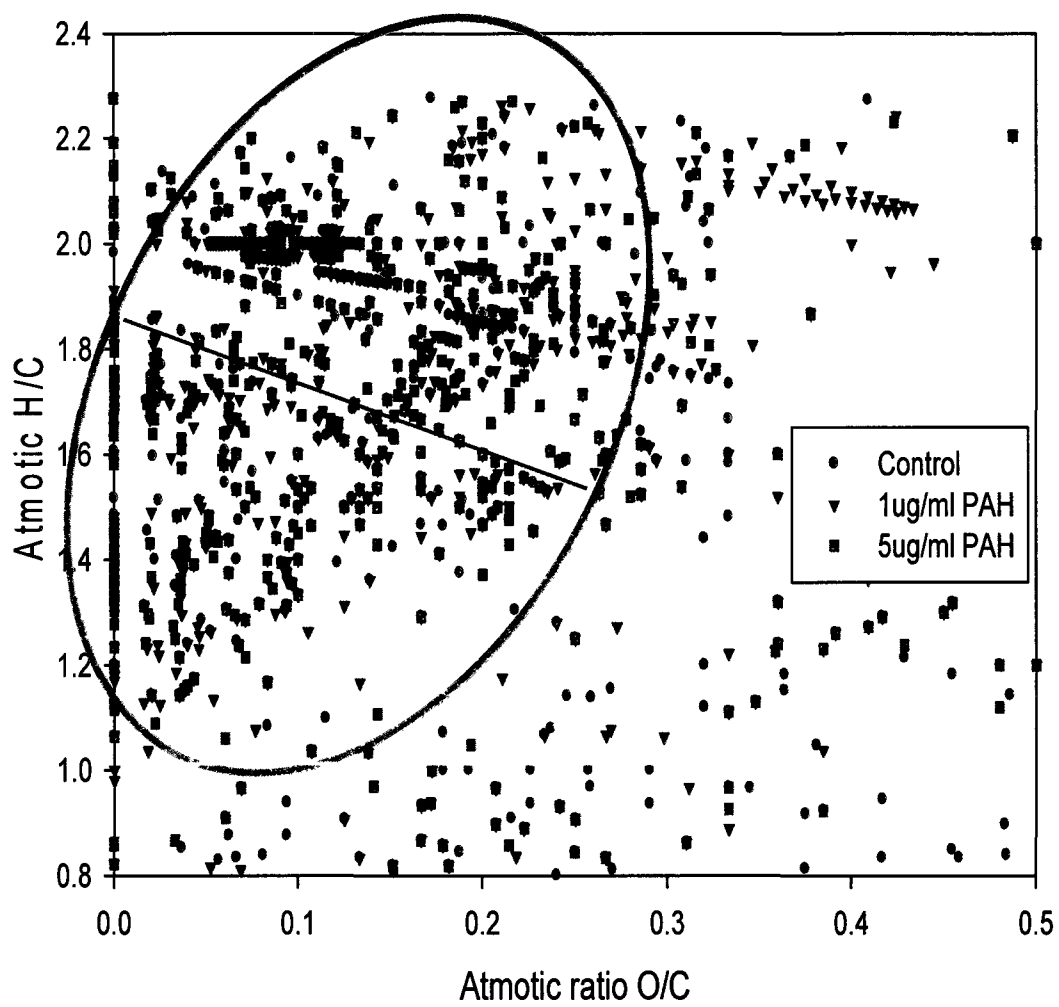
Figure 31. Lipid data plot in the van Krevelen diagram with the mole O/C and H/C rations between 0 and 0.4, and 1.5 and 2.2, respectively.

Since the van Krevenlen diagram failed to demonstrate the oxidative reaction, a new metric for the degree of oxidation of organic compounds, the average carbon oxidations state ($\overline{OSc}$) is used, which is a quantity that necessarily increases upon oxidation and is measurable using FT-ICR-MS. In the present study, the average carbon oxidations state coupled with carbon numbers (n_c) can provide a frame work for describing the insight into the oxidation. The oxidation state of carbon is defined by the identity and abundance of non-carbon atoms in the organic compounds; it may be simplified to

$$\overline{OSc} \approx 2\ O/C - H/C$$

The oxidation state of individual carbon atoms within a molecule may not change in the same way upon oxidation, but the average oxidation state of the carbon much increase (Kroll et al. 2011). Therefore, the quantity of average carbon oxidations state is an ideal metric for the degree of oxidation of lipids in this study.

Figure 32 showed the combinations of average carbon oxidation state and number of carbon atoms (n_c) for lipid molecules in HCAEC. In $\overline{OSc} \sim n_c$ space, lipid oxidation has an inherent directionality. Since the carbon oxidation state will increase upon oxidation, the ultimate end product is CO_2 (OSc = +4). Reaching this point requires both the addition of oxygen-containing moieties, which increases average carbon oxidations state ; and the breaking of C-C bonds, which decreases n_c. Thus, the blue arrows in Figure 33 indicate that the oxidation of HCAEC lipids involves an overall movement towards the upper right. This figure also represents three key classes of reactions: functionalization (the oxidative addition of polar functional groups to the

carbon skeleton), fragmentation (the oxidative cleavage of C-C bonds) and

oligomerization (the association of two organic molecules). Then possible combinations

of average carbon oxidation state and number of carbon atoms for lipid molecules in

Control, 1 and 5 µg/ml PAHs treated HCAEC are compared in figure 33. After PAHs

treatment, more plots are clustered with the $-2 < \overline{OSc} < -1$ (Figure 34), however, most

known compounds with higher average oxidation states are small, with 20-40 carbon

atoms.
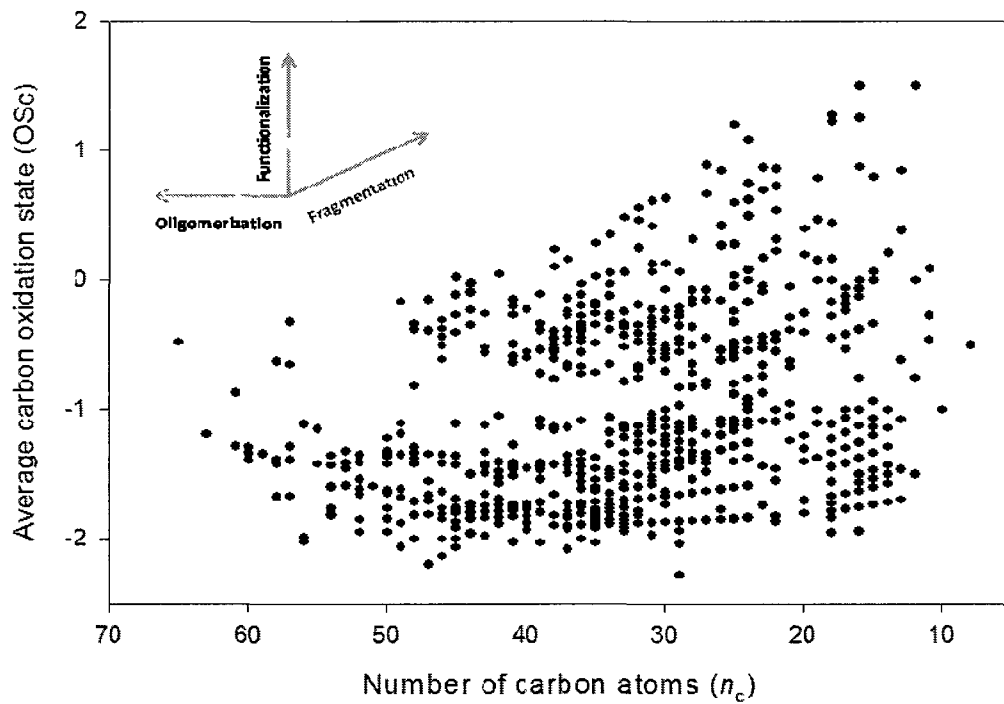
Figure 32. Possible combinations of average carbon oxidation state ($\overline{OSc}$) and number of carbon atoms (n_c) for lipid molecules in HCAEC.
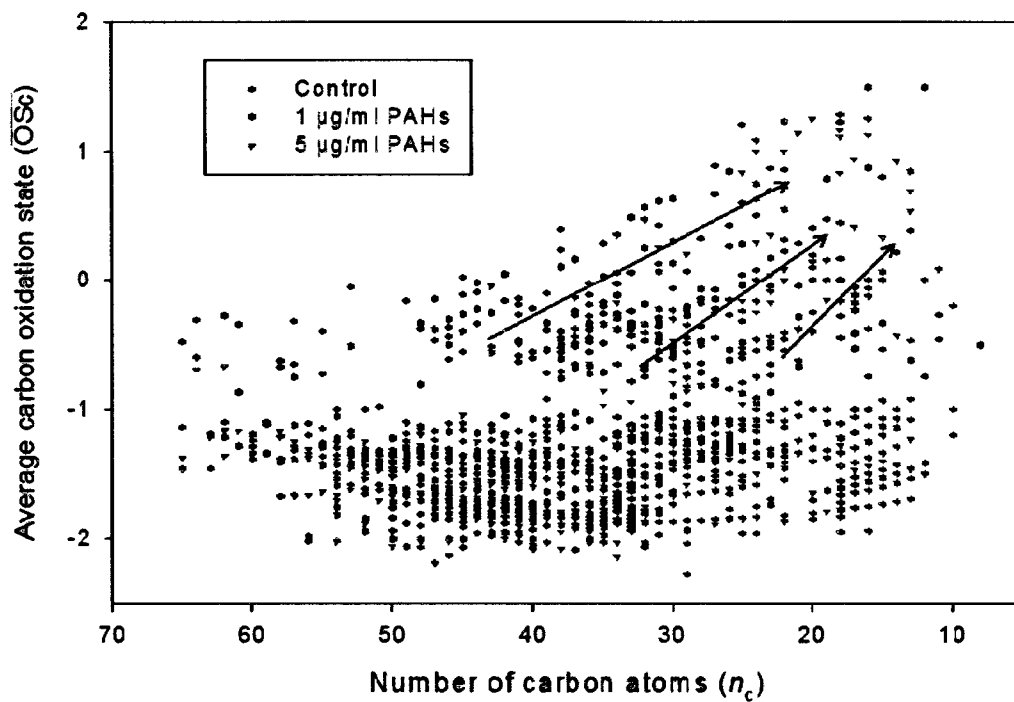
Figure 33. Possible combinations of average carbon oxidation state ($\overline{OSc}$) and number of carbon atoms (n_c) for lipid molecules in Control, 1 and 5 µg/ml PAHs treated HCAEC.
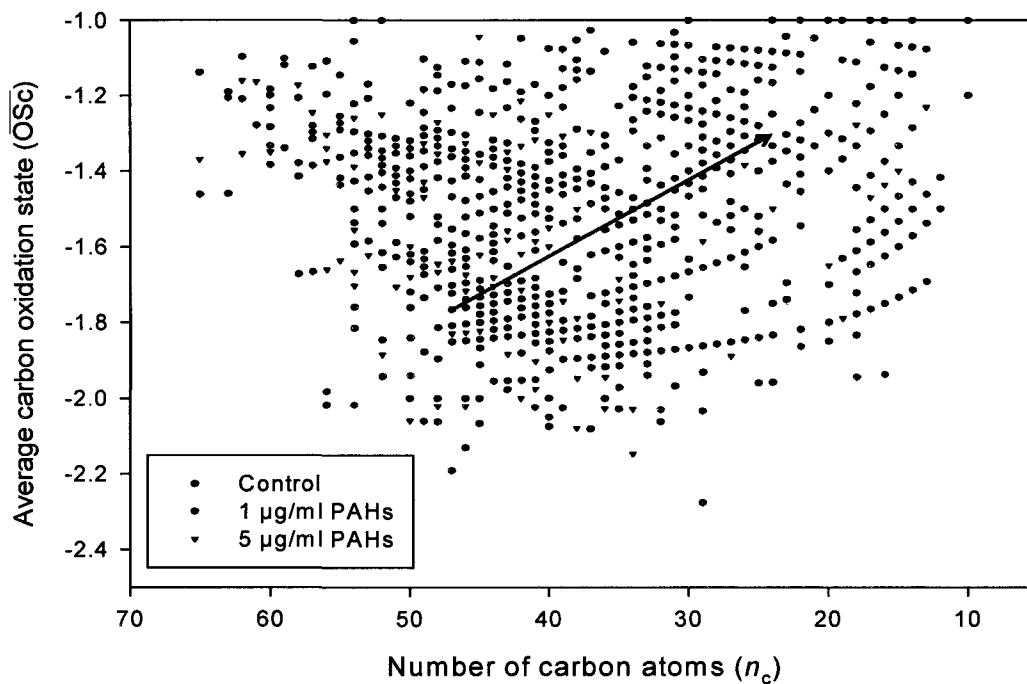
Figure 34. Possible combinations of average carbon oxidation state (- 2.5 $\leq$ $\overline{OSc}$ $\leq$ - 1.0) and number of carbon atoms (n_c) for lipid molecules in Control, 1 and 5 μg/ml PAHs treated HCAEC.

DISCUSSION

NO, a major signaling molecule has been shown to associate with oxidative stress and apoptosis in endothelial cells (Niu et al. 1994). It is also a key regulator of endothelial function generated by endothelial NO synthase (Forstermann et al. 1993). Vascular NO could relax blood vessels, prevent platelet aggregation and limit oxidation of low density lipoprotein cholesterol, decrease the expression of proinflammatory genes that advance atherogenesis (Forstermann 2008; Forstermann and Munzel 2006). Recent studies suggested that the toxicity of PAHs may be associated with NO level (Li et al. 2004). The present study documented the results of direct measurement of stimulated NO release from the HCAEC after short-term treatment with PAHs.

Total nitrite level from the PAHs treated cells was found to be increased than control. The higher level of NO release was found to be significantly increased after the treatment with 5 μg /ml of PAHs. NO released from these activated HCAEC along with the cell damage may thus regulate endothelial function. PAHs increased the NOS activity after 1 μg/ml, the magnitude of NO release was found to be greatly increased after 5 and 12 μg/ml concentration. These observations suggest that PAHs treatment causes eNOS up regulation after a short term exposure. Thus, these data clearly shows that, following PAHs treatment, eNOS was modulated within HCAEC that results inalteration of NO production. Similar findings have been reported in two studies that benzo[a]pyrene, a PAH compound, induced increased NO production in mouse neuroblastoma cells (Halliwell 2001; Dutta et al. 2010). The study demonstrated that PAHs induced lipid peroxidation in HCAEC as the evidence by the increased MDA production. MDA concentrations positively correlated with an increase in ROS

concentrations. 12T FT-ICR-MS was employed to detect lipids of HCAEC and the van Krevelen analysis was performed to depict lipid profiling. To our knowledge, this is the first study to examine the profile of the global lipid distribution in HCAEC in relation to PAH exposure. Based on the analysis of spectrum data in comparison to untreated groups, the van Krevelen analysis revealed a significant change in the lipid profile of the groups exposed to PAHs. The carbon oxidation state was employed to investigate the oxidation degree from the data of FT-ICR-MS. In the $\overline{OSc}$ - n_c space, oxidation moves HCAEC lipids upwards and to the right ($OSc = +4$, and $n_c = 1$), whereas radical association reactions in high oxygen environments. The measurement of average carbon oxidations state allows for the determination of the trajectories for entire lipid mixtures, offering the potential for lipids.

The number of lipid compounds increased after PAHs exposure, which is likely resulted from the oxidative stress. The increasing lipid species should be resulted from unsaturated fatty acyl side chain containing phospholipids, which were oxidized by ROS. The damage of endothelial cell membrane induced by PAHs may be the other reason to increase the number of lipid species by fragmentation.

In conclusion, PAHs were a group of components of PM that contributed to oxidative stress and the dysfunction of endothelial cells. In addition, PAHs contributed to lipid peroxidation and the changes in the global lipid profile of HCAEC after a short term exposure. This study has advanced the ability to identify lipids and to develop novel approaches applicable to large quantity sets of lipid molecular formula data.

CHAPTER IV

CONCLUSION

Epidemiologic studies have demonstrated a significant association between exposure to PM and atherosclerosis. Endothelial dysfunction and oxidative stress has been identified as a common denominator of many cardiovascular risk factors (Forstermann 2010). Thus, this study has investigated for the first time the role of PAHs in inducing vascular oxidative stress and endothelial dysfunction in HCAEC.

The findings of this study included the following:

- PM induced acute cytotoxicity to endothelial cells including change in cellular morphology, alteration of cellular membrane integrity, and decrease in cellular viability.

- PAHs were one of the major components in PM that contributed cytotoxicity to endothelial cells

- PAHs could induce a significant increase in ROS concentrations with resulting oxidative stress to endothelial cells.

- PAHs induced lipid peroxidation that can cause oxidative degradation of lipids, resulting in cell damage. .

- PAHs could alter the lipid profile of HCAEC and increase the number of lipid species.

- PAHs altered NO bioavailability by modulating eNOS activity after a short term exposure.

CHAPTER V

FUTURE STUDIES

The study showed that PAH induced a significant increase in the number of lipid specie from the global lipid profiling in HCAEC. The increasing lipid species should be resulted from unsaturated fatty acyl side chain containing phospholipids, which were oxidized by ROS. Therefore, the next steps beyond these preliminary data include identification of specific oxidized lipids, and investigate whether the oxidized lipids could serve as new candidates for oxidized lipid biomarkers.

In order to conclusively identify the pathway would require further investigation. The following pathways are considered to influence NO bioavailability as well; however, the related investigations will be conduct in this future: 1) A potential pathway for decomposition of NO is the rapid interaction with superoxide anions (O_2) to generate an oxidative stress maker, peroxynitrite (OONO) (Ignarro 2000). 2) Physical stimuli, receptor-dependent agonists will affect endothelium derived NO. 3) NO stimulates sGC that works to produce cGMP. The cGMP accumulation will disturb NO degradation in smooth muscle cells, and 4) thoroughly examine alteration of NO bioavailability observed in this study in relation to endothelial dysfunction.

REFERENCES

Alfaro-Moreno E, Martinez L, Garcia-Cuellar C, Bonner JC, Murray JC, Rosas I, et al. 2002. Biologic effects induced in vitro by PM10 from three different zones of Mexico City. Environ Health Perspect 110(7): 715-720.

Alfaro-Moreno E, Nawrot TS, Nemmar A, Nemery B. 2007. Particulate matter in the environment: pulmonary and cardiovascular effects. Curr Opin Pulm Med 13(2): 98-106.

Ashraf MZ, Kar NS, Podrez EA. 2009. Oxidized phospholipids: biomarker for cardiovascular diseases. Int J Biochem Cell Biol 41(6): 1241-1244.

Ashraf MZ, Kar NS, Podrez EA. 2009. Oxidized phospholipids: biomarker for cardiovascular diseases. Int J Biochem Cell Biol 41(6): 1241-1244.

ATSDR. 1995. Toxicological Profile for Polycyclic Aromatic Hydrocarbons (PAHs). Atlanta, GA. US Department of Health and Human Services, Public Health Service.

Bae S, Pan XC, Kim SY, Park K, Kim YH, Kim H, et al. 2010. Exposures to particulate matter and polycyclic aromatic hydrocarbons and oxidative stress in schoolchildren. Environ Health Perspect 118(4): 579-583.

Bai Y, Suzuki AK, Sagai M. 2001. The cytotoxic effects of diesel exhaust particles on human pulmonary artery endothelial cells in vitro: role of active oxygen species. Free Radic Biol Med 30(5): 555-562.

Bitar MS, Wahid S, Mustafa S, Al-Saleh E, Dhaunsi GS, Al-Mulla F. 2005. Nitric oxide dynamics and endothelial dysfunction in type II model of genetic diabetes. Eur J Pharmacol 511(1): 53-64.

Bonetti PO, Lerman LO, Lerman A. 2003. Endothelial dysfunction: a marker of atherosclerotic risk. Arterioscler Thromb Vasc Biol 23(2): 168-175.

Brown DM, Wilson MR, MacNee W, Stone V, Donaldson K. 2001. Size-dependent proinflammatory effects of ultrafine polystyrene particles: a role for surface area and oxidative stress in the enhanced activity of ultrafines. Toxicol Appl Pharmacol 175(3): 191-199.

Burcham PC. 1999. Internal hazards: baseline DNA damage by endogenous products of normal metabolism. Mutat Res 443(1-2): 11-36.

Chen LC, Nadziejko C. 2005. Effects of subchronic exposures to concentrated ambient particles (CAPs) in mice. V. CAPs exacerbate aortic plaque development in hyperlipidemic mice. Inhal Toxicol 17(4-5): 217-224.

Churg A, Brauer M. 1997. Human lung parenchyma retains PM2.5. Am J Respir Crit Care Med 155(6): 2109-2111.

Churg A, Brauer M. 2000. Ambient atmospheric particles in the airways of human lungs. Ultrastruct Pathol 24(6): 353-361.

Cruts B, van Etten L, Tornqvist H, Blomberg A, Sandstrom T, Mills NL, et al. 2008. Exposure to diesel exhaust induces changes in EEG in human volunteers. Part Fibre Toxicol 5: 4.

Davies KJ. 2000. Oxidative stress, antioxidant defenses, and damage removal, repair, and replacement systems. IUBMB Life 50(4-5): 279-289.

de Hartog JJ, Hoek G, Peters A, Timonen KL, Ibald-Mulli A, Brunekreef B, et al. 2003. Effects of fine and ultrafine particles on cardiorespiratory symptoms in elderly subjects with coronary heart disease: the ULTRA study. Am J Epidemiol 157(7): 613-623.

Delfino RJ, Sioutas C, Malik S. 2005. Potential role of ultrafine particles in associations between airborne particle mass and cardiovascular health. Environ Health Perspect 113(8): 934-946.

Desjardins F, Balligand JL. 2006. Nitric oxide-dependent endothelial function and cardiovascular disease. Acta Clin Belg 61(6): 326-334.

Domingues MR, Reis A, Domingues P. 2008. Mass spectrometry analysis of oxidized phospholipids. Chem Phys Lipids 156(1-2): 1-12.

Dutta K, Ghosh D, Nazmi A, Kumawat KL, Basu A. 2010. A common carcinogen benzo[a]pyrene causes neuronal death in mouse via microglial activation. PLoS One 5(4): e9984.

EPA. 1997. Particulate Matter (PM) – National Ambient Air Quality Standards.

EPA. 2004. Multi-Ethnic Study of Atherosclerosis (MESA) Air Pollution Study. US Environmental Protection Agency

EPA. 2008. Office of Solid Waste. Polycyclic Aromatic Hydrocarbons. Washington, DC.

Forstermann U. 2008. Oxidative stress in vascular disease: causes, defense mechanisms and potential therapies. Nat Clin Pract Cardiovasc Med 5(6): 338-349.

Forstermann U. 2010. Nitric oxide and oxidative stress in vascular disease. Pflugers Arch 459(6): 923-939.

Forstermann U, Munzel T. 2006. Endothelial nitric oxide synthase in vascular disease: from marvel to menace. Circulation 113(13): 1708-1714.

Forstermann U, Nakane M, Tracey WR, Pollock JS. 1993. Isoforms of nitric oxide synthase: functions in the cardiovascular system. Eur Heart J 14 Suppl I: 10-15.

Georgellis A, Toppari J, Veromaa T, Rydstrom J, Parvinen M. 1990. Inhibition of meiotic divisions of rat spermatocytes in vitro by polycyclic aromatic hydrocarbons. Mutat Res 231(2): 125-135.

Ghosh D, Mishra MK, Das S, Kaushik DK, Basu A. 2009. Tobacco carcinogen induces microglial activation and subsequent neuronal damage. J Neurochem 110(3): 1070-1081.

Gong KW, Zhao W, Li N, Barajas B, Kleinman M, Sioutas C, et al. 2007. Air-pollutant chemicals and oxidized lipids exhibit genome-wide synergistic effects on endothelial cells. Genome Biol 8(7): R149.

Goodarzi MT, Navidi AA, Rezaei M, Babahmadi-Rezaei H. 2010. Oxidative damage to DNA and lipids: correlation with protein glycation in patients with type 1 diabetes. J Clin Lab Anal 24(2): 72-76.

Gujral JS, Hinson JA, Farhood A, Jaeschke H. 2004. NADPH oxidase-derived oxidant stress is critical for neutrophil cytotoxicity during endotoxemia. Am J Physiol Gastrointest Liver Physiol 287(1): G243-252.

Guo Y, Jia Y, Pan X, Liu L, Wichmann HE. 2009. The association between fine particulate air pollution and hospital emergency room visits for cardiovascular diseases in Beijing, China. Sci Total Environ 407(17): 4826-4830.

Halliwell B. 2001. Role of free radicals in the neurodegenerative diseases: therapeutic implications for antioxidant treatment. Drugs Aging 18(9): 685-716.

Halliwell B. 2001. Role of free radicals in the neurodegenerative diseases: therapeutic implications for antioxidant treatment. Drugs Aging 18(9): 685-716.

Hein TW, Liao JC, Kuo L. 2000. oxLDL specifically impairs endothelium-dependent, NO-mediated dilation of coronary arterioles. Am J Physiol Heart Circ Physiol 278(1): H175-183.

Hesterberg TW, Bunn WB, 3rd, Chase GR, Valberg PA, Slavin TJ, Lapin CA, et al. 2006. A critical assessment of studies on the carcinogenic potential of diesel exhaust. Crit Rev Toxicol 36(9): 727-776.

Hesterberg TW, Bunn WB, 3rd, Chase GR, Valberg PA, Slavin TJ, Lapin CA, et al. 2006. A critical assessment of studies on the carcinogenic potential of diesel exhaust. Crit Rev Toxicol 36(9): 727-776.

Huang N, Ashrafpour H, Levine RH, Forrest CR, Neligan PC, Lipa JE, et al. 2010. Vasorelaxation Effect and Mechanism of Action of Vascular Endothelial Growth Factor-165 in Isolated Perfused Human Skin Flaps. J Surg Res.

Huang YC, Li Z, Harder SD, Soukup JM. 2004. Apoptotic and inflammatory effects induced by different particles in human alveolar macrophages. Inhal Toxicol 16(14): 863-878.

Hughey CA, Hendrickson CL, Rodgers RP, Marshall AG, Qian K. 2001. Kendrick mass defect spectrum: a compact visual analysis for ultrahigh-resolution broadband mass spectra. Anal Chem 73(19): 4676-4681.

Ichinose T, Furuyama A, Sagai M. 1995. Biological effects of diesel exhaust particles (DEP). II. Acute toxicity of DEP introduced into lung by intratracheal instillation. Toxicology 99(3): 153-167.

Ignarro LJ. 2000. The unique role of nitric oxide as a signaling molecule in the cardiovascular system. Ital Heart J 1 Suppl 3: S28-29.

Ivanova PT, Cerda BA, Horn DM, Cohen JS, McLafferty FW, Brown HA. 2001. Electrospray ionization mass spectrometry analysis of changes in phospholipids in RBL-2H3 mastocytoma cells during degranulation. Proc Natl Acad Sci U S A 98(13): 7152-7157.

Jeng HA, Pan CH, Diawara N, Chang-Chien GP, Lin WY, Huang CT, et al. 2010. Polycyclic aromatic hydrocarbon-induced oxidative stress and lipid peroxidation in relation to immunological alteration. Occup Environ Med.

Jones JJ, Batoy SM, Wilkins CL. 2005. A comprehensive and comparative analysis for MALDI FTMS lipid and phospholipid profiles from biological samples. Comput Biol Chem 29(4): 294-302.

Kang JJ, Cheng YW. 1997. Polycyclic aromatic hydrocarbons-induced vasorelaxation through activation of nitric oxide synthase in endothelium of rat aorta. Toxicol Lett 93(1): 39-45.

Kavouras IG, Stephanou EG. 2002. Gas/particle partitioning and size distribution of primary and secondary carbonaceous aerosols in public buildings. Indoor Air 12(1): 17-32.

Kavouras IG, Stephanou EG. 2002. Gas/particle partitioning and size distribution of primary and secondary carbonaceous aerosols in public buildings. Indoor Air 12(1): 17-32.

Kim S, Kramer RW, Hatcher PG. 2003. Graphical method for analysis of ultrahigh-resolution broadband mass spectra of natural organic matter, the van Krevelen diagram. Anal Chem 75(20): 5336-5344.

Konorev EA, Zhang H, Joseph J, Kennedy MC, Kalyanaraman B. 2000. Bicarbonate exacerbates oxidative injury induced by antitumor antibiotic doxorubicin in cardiomyocytes. Am J Physiol Heart Circ Physiol 279(5): H2424-2430.

Kroll JH, Donahue NM, Jimenez JL, Kessler SH, Canagaratna MR, Wilson KR, et al. 2011. Carbon oxidation state as a metric for describing the chemistry of atmospheric organic aerosol. Nat Chem 3(2): 133-139.

Kunzli N, Jerrett M, Mack WJ, Beckerman B, LaBree L, Gilliland F, et al. 2005. Ambient air pollution and atherosclerosis in Los Angeles. Environ Health Perspect 113(2): 201-206.

Laden F, Schwartz J, Speizer FE, Dockery DW. 2006. Reduction in fine particulate air pollution and mortality: Extended follow-up of the Harvard Six Cities study. Am J Respir Crit Care Med 173(6): 667-672.

Li CH, Lee CC, Cheng YW, Juang HA, Kang JJ. 2004. Activation and up-regulation of nitric oxide synthase in human umbilical vein endothelial cells by polycyclic aromatic hydrocarbons. Toxicol Lett 151(2): 367-374.

Li CH, Lee CC, Cheng YW, Juang HA, Kang JJ. 2004. Activation and up-regulation of nitric oxide synthase in human umbilical vein endothelial cells by polycyclic aromatic hydrocarbons. Toxicol Lett 151(2): 367-374.

Li N, Sioutas C, Cho A, Schmitz D, Misra C, Sempf J, et al. 2003. Ultrafine particulate pollutants induce oxidative stress and mitochondrial damage. Environ Health Perspect 111(4): 455-460.

Li N, Xia T, Nel AE. 2008. The role of oxidative stress in ambient particulate matter-induced lung diseases and its implications in the toxicity of engineered nanoparticles. Free Radic Biol Med 44(9): 1689-1699.

Libby P, Ridker PM, Maseri A. 2002. Inflammation and atherosclerosis. Circulation 105(9): 1135-1143.

Limoli CL, Kaplan MI, Giedzinski E, Morgan WF. 2001. Attenuation of radiation-induced genomic instability by free radical scavengers and cellular proliferation. Free Radic Biol Med 31(1): 10-19.

Liu L, Ruddy T, Dalipaj M, Poon R, Szyszkowicz M, You H, et al. 2009. Effects of indoor, outdoor, and personal exposure to particulate air pollution on cardiovascular physiology and systemic mediators in seniors. J Occup Environ Med 51(9): 1088-1098.

Lubos E, Handy DE, Loscalzo J. 2008. Role of oxidative stress and nitric oxide in atherothrombosis. Front Biosci 13: 5323-5344.

Lunch A. 2005. The Carcinogenic Effects of Polycyclic Aromatic Hydrocarbons. . London: Imperial College Press.

Mates JM, Sanchez-Jimenez FM. 2000. Role of reactive oxygen species in apoptosis: implications for cancer therapy. Int J Biochem Cell Biol 32(2): 157-170.

Meerson FZ, Kagan VE, Kozlov Yu P, Belkina LM, Arkhipenko Yu V. 1982. The role of lipid peroxidation in pathogenesis of ischemic damage and the antioxidant protection of the heart. Basic Res Cardiol 77(5): 465-485.

Miller KA, Siscovick DS, Sheppard L, Shepherd K, Sullivan JH, Anderson GL, et al. 2007. Long-term exposure to air pollution and incidence of cardiovascular events in women. N Engl J Med 356(5): 447-458.

Montiel-Davalos A, Ibarra-Sanchez Mde J, Ventura-Gallegos JL, Alfaro-Moreno E, Lopez-Marure R. 2010. Oxidative stress and apoptosis are induced in human endothelial cells exposed to urban particulate matter. Toxicol In Vitro 24(1): 135-141.

Niu XF, Smith CW, Kubes P. 1994. Intracellular oxidative stress induced by nitric oxide synthesis inhibition increases endothelial cell adhesion to neutrophils. Circ Res 74(6): 1133-1140.

O'Donnell VB, Freeman BA. 2001. Interactions between nitric oxide and lipid oxidation pathways: implications for vascular disease. Circ Res 88(1): 12-21.

Ohtani K, Egashira K. 2004. [NO and atherosclerosis]. Nippon Rinsho 62 Suppl 9: 544-547.

Oksvold MP, Skarpen E, Widerberg J, Huitfeldt HS. 2002. Fluorescent histochemical techniques for analysis of intracellular signaling. J Histochem Cytochem 50(3): 289-303.

Peters A, Wichmann HE, Tuch T, Heinrich J, Heyder J. 1997. Respiratory effects are associated with the number of ultrafine particles. Am J Respir Crit Care Med 155(4): 1376-1383.

Polichetti G, Cocco S, Spinali A, Trimarco V, Nunziata A. 2009. Effects of particulate matter (PM(10), PM(2.5) and PM(1)) on the cardiovascular system. Toxicology 261(1-2): 1-8.

Pope CA, 3rd, Dockery DW. 2006. Health effects of fine particulate air pollution: lines that connect. J Air Waste Manag Assoc 56(6): 709-742.

Prasad MR. 1991. Endothelin stimulates degradation of phospholipids in isolated rat hearts. Biochem Biophys Res Commun 174(2): 952-957.

Protection. R. Regulations (Standards-29 CFR). Personal Protective Equipment. Occupational Safety and Health Standards 1910.134.

Rajagopalan S, Sun Q, Chen LC. 2005. Particulate pollution and endothelial function: deja vu all over again in the air. Circulation 111(22): 2869-2871.

RESTEK. 2010. EPA method 8310 PAH mixture. Material Safety Data Sheet.

Rudolph V, Freeman BA. 2009. Cardiovascular consequences when nitric oxide and lipid signaling converge. Circ Res 105(6): 511-522.

Saghatelian A, Trauger SA, Want EJ, Hawkins EG, Siuzdak G, Cravatt BF. 2004. Assignment of endogenous substrates to enzymes by global metabolite profiling. Biochemistry 43(45): 14332-14339.

Salganik RI. 2001. The benefits and hazards of antioxidants: controlling apoptosis and other protective mechanisms in cancer patients and the human population. J Am Coll Nutr 20(5 Suppl): 464S-472S; discussion 473S-475S.

Salvi S, Holgate ST. 1999. Mechanisms of particulate matter toxicity. Clin Exp Allergy 29(9): 1187-1194.

Salvi S, Holgate ST. 1999. Mechanisms of particulate matter toxicity. Clin Exp Allergy 29(9): 1187-1194.

Samii J. 2003. Endothelial cell lipid peroxidation impairs nitric oxide bioactivity. Dissertation.

Sanders LM. 2005. Effects of dietary fat and fiber on the oxidative status of the small intestine and colon of rats. Dissertation.

Schneider A, Neas L, Herbst MC, Case M, Williams RW, Cascio W, et al. 2008. Endothelial dysfunction: associations with exposure to ambient fine particles in diabetic individuals. Environ Health Perspect 116(12): 1666-1674.

Schneider A, Neas L, Herbst MC, Case M, Williams RW, Cascio W, et al. 2008. Endothelial dysfunction: associations with exposure to ambient fine particles in diabetic individuals. Environ Health Perspect 116(12): 1666-1674.

Schwartz J. 1999. Air pollution and hospital admissions for heart disease in eight U.S. counties. Epidemiology 10(1): 17-22.

Schwartz J. 2001. Is there harvesting in the association of airborne particles with daily deaths and hospital admissions? Epidemiology 12(1): 55-61.

Shaul PW. 2003. Endothelial nitric oxide synthase, caveolae and the development of atherosclerosis. J Physiol 547(Pt 1): 21-33.

Simkhovich BZ, Kleinman MT, Kloner RA. 2008. Air pollution and cardiovascular injury epidemiology, toxicology, and mechanisms. J Am Coll Cardiol 52(9): 719-726.

Sleighter RL, Hatcher PG. 2007. The application of electrospray ionization coupled to ultrahigh resolution mass spectrometry for the molecular characterization of natural organic matter. J Mass Spectrom 42(5): 559-574.

Sorensen M, Daneshvar B, Hansen M, Dragsted LO, Hertel O, Knudsen L, et al. 2003. Personal PM2.5 exposure and markers of oxidative stress in blood. Environ Health Perspect 111(2): 161-166.

Stenson AC, Marshall AG, Cooper WT. 2003. Exact masses and chemical formulas of individual Suwannee River fulvic acids from ultrahigh resolution electrospray ionization Fourier transform ion cyclotron resonance mass spectra. Anal Chem 75(6): 1275-1284.

Sun Q, Wang A, Jin X, Natanzon A, Duquaine D, Brook RD, et al. 2005. Long-term air pollution exposure and acceleration of atherosclerosis and vascular inflammation in an animal model. JAMA 294(23): 3003-3010.

Sydbom A, Blomberg A, Parnia S, Stenfors N, Sandstrom T, Dahlen SE. 2001. Health effects of diesel exhaust emissions. Eur Respir J 17(4): 733-746.

Uittenbogaard A, Shaul PW, Yuhanna IS, Blair A, Smart EJ. 2000. High density lipoprotein prevents oxidized low density lipoprotein-induced inhibition of endothelial nitric-oxide synthase localization and activation in caveolae. J Biol Chem 275(15): 11278-11283.

van Eeden SF, Yeung A, Quinlam K, Hogg JC. 2005. Systemic response to ambient particulate matter: relevance to chronic obstructive pulmonary disease. Proc Am Thorac Soc 2(1): 61-67.

Wells PG, Kim PM, Laposa RR, Nicol CJ, Parman T, Winn LM. 1997. Oxidative damage in chemical teratogenesis. Mutat Res 396(1-2): 65-78.

Wexler P. 2005. Encyclopedia of Toxicology(Second Edition). Elsevier Inc.

WHO. 2003. Health Aspects of Air Pollution with Particulate Matter, Ozone and Nitrogen Dioxide. World Health Organization Boon, Germany. 1-94.

Widlansky ME, Gokce N, Keaney JF, Jr., Vita JA. 2003. The clinical implications of endothelial dysfunction. J Am Coll Cardiol 42(7: 1149-1160.

Wiemer G, Linz W, Hatrik S, Scholkens BA, Malinski T. 1997. Angiotensin-converting enzyme inhibition alters nitric oxide and superoxide release in normotensive and hypertensive rats. Hypertension 30(5): 1183-1190.

Wiseman H, Halliwell B. 1996. Damage to DNA by reactive oxygen and nitrogen species: role in inflammatory disease and progression to cancer. Biochem J 313 (Pt 1)A: 17-29.

Woodruff TJ, Darrow LA, Parker JD. 2008. Air pollution and postneonatal infant mortality in the United States, 1999-2002. Environ Health Perspect 116(1): 110-115.

Yu ea. 2006. Identification of Phospholipid Molecular Species in Porcine Brain Extracts Using High Mass Accuracy of 4.7 Tesla Fourier Transform Ion Cyclotron Resonance Mass Spectrometry. Bull Korean Chem Soc 27(5): 793-796.

Zanobetti A, Schwartz J. 2005. The effect of particulate air pollution on emergency admissions for myocardial infarction: a multicity case-crossover analysis. Environ Health Perspect 113(8): 978-982.

APPENDICES

APPENDIX A

CERTIFIED CONCENTRATIONS FRO SELESTED PAHS IN SRM 2975

	Mass Fractions (mg kg)[a]		
Phenanthrene[a,c,d,e,f,g]	17 0	±	2 8
Fluoranthene[b,c,d,e,f,g]	26 6	±	5 1
Pyrene[b,c,d,e,f,g]	0 90	±	0 24
Benz[a]anthracene[c,d,e,f,g,a]	0.317	±	0 066
Chrysene[f,a]	4 56	±	0 16
Triphenylene[g,b]	5 22	±	0 20
Benzo[j]fluoranthene[c,e]	0 82	±	0 11
Benzo[k]fluoranthene[c,d,e,f,g,a]	0 678	±	0 076
Benzo[e]pyrene[b,c,d,e,f,h]	1 11	±	0 10
Benzo[a]pyrene[e,f,g,h]	0 222	±	0 053
Benzo[g,h]perylene[b,c,e,f]	0 498	±	0 044

[a] Each set of results is expressed as the certified value ± the expanded uncertainty. Each certified value is a mean of the means from two or more analytical methods. For results from two methods the certified value is the equally weighted mean for results from three or more methods the certified value is the mean weighted as described in Paule and Mandel [19]. Each uncertainty computed according to the CIPM approach as described in the ISO and NIST Guides [3] is an expanded uncertainty at the 95 % level of confidence which includes random sources of uncertainty within each analytical method and among methods as well as uncertainty due to the variation among the bottles. The expanded uncertainty defines a range of values within which the true value is believed to lie at a level of confidence of approximately 95 %.

[b] GC MS (Ia) on 5 % phenyl-substituted methylpolysiloxane phase after PFE with toluene methanol mixture. GC MS (Ib) on 5 % phenyl-substituted methylpolysiloxane phase after PFE with DCM

[c] GC MS (III) on 5 % phenyl-substituted methylpolysiloxane phase after Soxhlet extraction with DCM

[d] GC MS (IVa) on 5 % phenyl-substituted methylpolysiloxane phase after PFE with DCM

[e] GC MS (IVb) on 50 % phenyl-substituted methylpolysiloxane phase of same extracts as GC MS (IVa)

[f] LC-FL of isomeric PAH fractions after Soxhlet extraction with DCM

[g] GC MS (IVc) on a smectic liquid crystalline phase of same extracts as GC MS (IVa)

[h] GC MS (Ib) on 50 % phenyl-substituted methylpolysiloxane phase of selected extracts from GC MS (Ia)

APPENDIX B

REFERENCE CONCENTRATIONS FRO SELECTED PAHS IN SRM 2975

	Mass Fractions (mg kg)[a]		
1-Methylphenanthrene[b,c,d,e,f]	0.89	±	0.11
2-Methylphenanthrene[b,c,d,e,f]	2.0	±	0.2
3-Methylphenanthrene[b,c,d,e,f]	1.0	±	0.2
4- and 9-Methylphenanthrene[b,c,d,e,f]	0.44	±	0.09
1,2-Dimethylphenanthrene[a,f]	0.05	±	0.02
1,6-, 1,7-, 2,5-, and 2,9-Dimethylphenanthrene[a,f]	0.57	±	0.08
1,8-Dimethylphenanthrene[a,f]	0.60	±	0.02
2,6-Dimethylphenanthrene[a,f]	0.25	±	0.05
2,7-Dimethylphenanthrene[a,f]	0.23	±	0.05
3,6-Dimethylphenanthrene[a,f]	0.18	±	0.02
Anthracene[a,g]	0.038	±	0.008
Benzo[ghi]fluoranthene[b]	10.2	±	0.5
8-Methylfluoranthene[f]	0.068	±	0.004
1-, 3-, and 7-Methylfluoranthene[e]	0.53	±	0.03
2-Methylpyrene[a,f]	0.040	±	0.008
4-Methylpyrene[a,f]	0.022	±	0.005
Benzo[c]phenanthrene[b,c,d,e,f,h]	1.0	±	0.4
Benzo[a]fluoranthene[f]	0.06	±	0.02
Benzo[b]fluoranthene[c,h,i]	11.5	±	3.6
Perylene[g]	0.054	±	0.009
Indeno[1,2,3-cd]pyrene[a,f]	1.4	±	0.2
Indeno[1,2,3-c,f]fluoranthene[f]	1.1	±	0.2
Dibenz[a,j]anthracene[e]	0.37	±	0.07
Dibenz[a,c]anthracene Dibenz[a,h]anthracene[a]	0.52	±	0.08
Pentaphene[e]	0.038	±	0.007
Benzo[b]chrysene[a,f]	0.08	±	0.03
Picene[a,f]	1.0	±	0.2
Coronene[e]	1.1	±	0.2

[a] Each set of results is expressed as the reference value ± the expanded uncertainty. Each reference value is the mean from one analytical method or a mean of the means from two or more analytical methods. For results from two methods, the certified value is the equally weighted mean; for results from three or more methods, the certified value is the mean weighted as described in Paule and Mandel [19]. Each uncertainty, computed according to the CIPM approach as described in the ISO and NIST Guides [3] is an expanded uncertainty at the 95 % level of confidence which includes random sources of uncertainty within each analytical method and among methods, as well as uncertainty due to the variation among the bottles. The expanded uncertainty defines a range that contains the estimate of the true value at a level of confidence of approximately 95 %.

[b] GC MS (Ia) on 5 % phenyl-substituted methylpolysiloxane phase after PFE with toluene methanol mixture

[c] GC MS (II) on 5 % phenyl-substituted methylpolysiloxane phase after PFE with DCM

[d] GC MS (III) on 5 % phenyl-substituted methylpolysiloxane phase after Soxhlet extraction with DCM

[e] GC MS (IVa) on 5 % phenyl-substituted methylpolysiloxane phase after PFE with DCM

[g] GC MS (IVb) on 50 % phenyl-substituted methylpolysiloxane phase of same extracts as GC MS (IVa)

[f] LC-FL of isomeric PAH fractions after Soxhlet extraction with DCM

[h] GC MS (IVc) on a smectic liquid crystalline phase of same extracts as GC MS (IVa)

[i] GC MS (Ib) on 50 % phenyl-substituted methylpolysiloxane phase of selected extracts from GC MS (Ia)

APPENDIX C

REFERENCE VALUES FOR PARTICLE-SIZE CHARACTERISTICS FOR SRM 2975

Particle Measurement	Value[a]		
Mean diameter (volume distribution, MV, μm)[c]	31 9	±	0 6
Mean diameter (area distribution, μm)[c]	11 2	±	0 1
Mean diameter (number distribution, μm)[d]	1 62	±	0 01
Surface Area (m^2/cm^3)[e]	0 538	±	0 006

The following data show the percent of the volume that is smaller than the indicated size

Percentile	Particle Diameter (μm)[a]		
95	110	±	3
90	70	±	2
80	44 9	±	0 8
70	32 4	±	0 6
60	24 8	±	0 4
50[f]	19 4	±	0 3
40	15 2	±	0 2
30	11 7	±	0 2
20	8 5	±	0.1
10	5 3	±	0 1

[a] Each reference value is the mean value of measurements from the analysis of subsamples from four bottles. Each uncertainty computed according to the CIPM approach as described in the NIST and ISO Guides [3], is an expanded uncertainty at the 95 % level of confidence. The expanded uncertainty defines a range that contains the best estimate of the true value at a level of confidence of approximately approximately 95 %.

[b] The mean diameter of the volume distribution represents the center of gravity of the distribution and compensates for scattering efficiency and refractive index. This parameter is strongly influenced by coarse particles

[c] The mean diameter of the area distribution calculated from the volume distribution with less influence from the presence of coarse particles than the MV parameter

[d] The mean diameter of the number distribution calculated from the volume distribution

[e] Calculated specific surface area assuming solid spherical particles. This is a computation and should not be interchanged with an adsorption method of surface area determination (see Table 6) as this value does not reflect porosity or topographical characteristics

[f] Median diameter (50 % of the volume is less than 19 4 μm)

APPENDIX D

CERTIFICATE OF EPA METHOD 8310 PAH MIXTURE

Elution Order	Compound	CAS #	Percent Purity [2]	Concentration [3] (weight/volume)	% Uncertainty [4] (95% C.L.; K=2)
1	Naphthalene	91-20-3	95%	500 000 ug/ml	±0.59%
2	1 Methylnaphthalene	90-12-0	95%	500 000 ug/ml	±0.59%
3	2 Methylnaphthalene	91-57-6	97%	499 550 ug/ml	±0.59%
4	Acenaphthylene	208-96-8	99%	50 000 ug/ml	±0.59%
5	Acenaphthene	83-32-9	99%	500 000 ug/ml	±0.59%
6	Fluorene	86-73-7	98%	500 000 ug/ml	±0.59%
7	Phenanthrene	85-01-8	98%	500 000 ug/ml	±0.59%
8	Anthracene	120-12-7	98%	500 000 ug/ml	±0.59%
9	Fluoranthene	206-44-0	98%	499 800 ug/ml	±0.59%
10	Pyrene	129-00-0	98%	499 800 ug/ml	±0.59%
11	Benz[a]anthracene	56-55-3	98%	500 000 ug/ml	±0.59%
12	Chrysene	218-01-9	99%	500 000 ug/ml	±0.59%
13	Benzo[b]fluoranthene	205-99-2	99%	500 000 ug/ml	±0.59%
14	Benzo[k]fluoranthene	207-08-9	99%	500 000 ug/ml	±0.59%
15	Benzo[a]pyrene	50-32-8	98%	500 000 ug/ml	±0.59%
16	Indeno[1,2,3-cd]pyrene	193-39-5	99%	500 000 ug/ml	±0.59%
17	Dibenz[a,h]anthracene	53-70-3	99%	500 000 ug/ml	±0.59%
18	Benzo[g,h,i]perylene	191-24-2	90%	500 000 ug/ml	±0.59%
Solvent:	Acetonitrile	75-05-8	99%		

APPENDIX E

LIST OF ABBREVIATIONS

Abbreviations	The full names
A23187	Calcium ionosphore
ANOVA	Analysis of variance
BSA	Bovine serum albumin
Carboxy-H_2DFFDA	5-(and-6)-carboxy-2', 7'- difluorodihydrofluorescein diacetate
cGMP	3', 5'- guanosine monophosphate
CVDs	Cardiovascular diseases
DAF-2DA	4, 5 Diaminofluorescein diacetate
DAF-2T	Triazolofluorescein
DCF	2', 7'-dichlorodihydrofluorescein
DFF	2', 7'- difluorodihydrofluorescein
DMSO	Dimethyl sulfoxide
DLS	Dynamic light scattering
DPI	Diphenyleneiodonium chloride
DPM	Diesel particulate matter
EDRF	Endothelium-derived relaxing factor
EDTA	Ethylenediaminetetraacetic acid
EGTA	Ethylene glycol tetraacetic acid
eNOS	Endothelial nitric oxide synthase

LIST OF ABBREVIATIONS

FBS	Fetal bovine serum
Fe^{2+}	Ferrous iron
Fe^{3+}	Ferric iron
FMD	Flow-medicated dilation
FT-ICR-MS	Fourier transform ion cyclotron resonance mass spectrometry
ET-1	Endothelin -1
HBSS	Hank's Buffered Salt Solution
HCAEC	Human coronary artery endothelial cells
H_2DCFDA	2', 7'-dichlorodihydrofluorescein diacetate
H_2DFFDA	2', 7'- difluorodihydrofluorescein diacetate
H_2O_2	Hydrogen peroxide
iNOS	Inducible nitric oxide synthase
IL-1ß	Interleukin-1ß
IL-6	Interleukin-6
IL-8	Interleukin-8
LDH	Lactate dehydrogenase
L-NAME	N^w-nitro-L-arginine methyl ester hydrochloride
LPO	Lipid peroxidation
MDA	Malondialdehyde

LIST OF ABBREVIATIONS

NF κB	Nuclear factor kappa-B
nNOS	Neuronal nitric oxide synthase
NO	Nitric Oxide
NO^{2-}	Nitrite
NO^{3-}	Nitrate
$ONOO^{-}$	Peroxynitrite
oxLDL	Oxidative low-density lipoprotein
PAHs	Poly-aromatic Hydrocarbons
PM	Particulate matters
$PM_{2.5}$	Particulate matter with diameter under 2.5 μm
PM_{10}	Particulate matter with diameter under 10 μm
PUFA	Polyunsaturated fatty acid
ROS	Reactive oxygen species
SEM	Standard error of the mean
SEM-EDS	Scanning Electron Microscopy- Energy Dispersive Spectroscopy
TBARS	Thiobarbituric acid reactive substances
UFP	Ultrafine particle, particulate matter with diameter under 0.1 μm

VITA

Address

Department of Biology, College of Science, Old Dominion University, Norfolk, VA

Education

Ph.D. in Biomedical Sciences, Old Dominion University, Norfolk, VA (August 2011)

M.S., B.S. in Biosciences, Beijing Institute of Technology, China (July 2006)

Honors and Awards

Biology Graduate Student Research Award, Old Dominion University, 2011

Graduate Travel Award, Association of Southern Biologists, 2010-2011

Graduate Fellowship, National Institute for Occupational Safety and Health, 2010

Membership in Scholarly Societies

- American Heart Association
- Association of Southern Biologists
- American Public Health Association
- Society of Toxicology

Publications and Conference Presentations

Yu L, Mazzer P, et al. Poster: "Effects of polycyclic aromatic hydrocarbons on lipid profile and nitric oxide level in vascular endothelial cells", Arteriosclerosis, Thrombosis and Vascular Biology Scientific Sessions. Chicago, IL, April 2011

Yu L, "Polycyclic aromatic hydrocarbons in particulate matter alter lipid profile in human endothelial cells", Society of Toxicology Annual Meeting. Washington D.C. March 2011

Jeng HA, **Yu L**, "Alteration of sperm quality and hormone levels by polycyclic aromatic hydrocarbons on airborne particulate particles", *Journal of Environmental Science and Health, Part A.*, June 2008, 43(7), 675-681